

2018

## Application of Box-Behnken Experimental Design for the Formulation and Optimisation of Selenomethionine-Loaded Chitosan Nanoparticles Coated with Zein for Oral Delivery.

Giuliana Vozza

*Technological University Dublin*

Minna Danish

*Technological University Dublin*

Hugh Byrne

*Technological University Dublin, hugh.byrne@tudublin.ie*

*See next page for additional authors*

Follow this and additional works at: <https://arrow.tudublin.ie/nanolart>

 Part of the [Physics Commons](#)

### Recommended Citation

Ryan, S. et al. (2018) Application of Box-Behnken Experimental Design for the Formulation and Optimisation of Selenomethionine-Loaded Chitosan Nanoparticles Coated with Zein for Oral Delivery, *Int J Pharm.* 2018 Nov 15;551(1-2):257-269. doi:10.1016/j.ijpharm.2018.08.050

This Article is brought to you for free and open access by the NanoLab at ARROW@TU Dublin. It has been accepted for inclusion in Articles by an authorized administrator of ARROW@TU Dublin. For more information, please contact [arrow.admin@tudublin.ie](mailto:arrow.admin@tudublin.ie), [aisling.coyne@tudublin.ie](mailto:aisling.coyne@tudublin.ie), [vera.kilshaw@tudublin.ie](mailto:vera.kilshaw@tudublin.ie).



This work is licensed under a [Creative Commons Attribution-NonCommercial-Share Alike 4.0 International License](#).

---

## Authors

Giuliana Vozza, Minna Danish, Hugh Byrne, Jesus Maria Frias, and Sinéad M. Ryan

1 **Application of Box-Behnken experimental design for the formulation and**  
2 **optimisation of selenomethionine-loaded chitosan nanoparticles coated with**  
3 **zein for oral delivery**

4  
5 Giuliana Vozza<sup>a,b</sup>, Minna Danish<sup>a,b</sup>, Hugh J. Byrne<sup>b</sup>, Jesús M. Frías<sup>c</sup>, Sinéad M. Ryan<sup>d,\*</sup>

6 <sup>a</sup> School of Food Science and Environmental Health, Dublin Institute of Technology,

7 Marlborough Street, Dublin 1, Ireland

8 <sup>b</sup> FOCAS Research Institute, Dublin Institute of Technology, Kevin Street, Dublin 8, Ireland

9 <sup>c</sup> Environmental Science and Health Institute, Dublin Institute of Technology, Grangegorman,

10 <sup>d</sup> School of Veterinary Medicine, University College Dublin, Belfield, Dublin 4, Ireland

11 Dublin 7, Ireland

12 \* Corresponding author. E-mail: [Sinead.Ryan@ucd.ie](mailto:Sinead.Ryan@ucd.ie)

13

14

15

16

17

18

19

20

21

22

23

24

25

26 **Abstract:**

27 Selenomethionine is an essential amino acid with a narrow therapeutic index and  
28 susceptibility to oxidation. Here it was encapsulated into a nanoparticle composed of chitosan  
29 cross-linked with tripolyphosphate for oral delivery. The formulation was optimised using a  
30 three-factor Box-Behnken experimental design. The chitosan:tripolyphosphate ratio, chitosan  
31 solvent pH, and drug load concentration were independently varied. The dependent variables  
32 studied were encapsulation efficiency, particle size, polydispersity index and zeta potential.  
33 For optimisation, encapsulation efficiency and zeta potential were maximised, particle  
34 diameter was set to 300 nm and polydispersity index was minimised. A 0.15mg/mL  
35 concentration of selenomethionine, chitosan solvent pH of 3, and chitosan:tripolyphosphate  
36 ratio of 6:1 yielded optimum nanoparticles of size  $187\pm 58$ nm, polydispersity index  
37  $0.24\pm 0.01$ , zeta potential  $36\pm 6$ mV, and encapsulation efficiency of  $39\pm 3\%$ . Encapsulation  
38 efficiency was doubled to  $80\pm 1.5\%$  by varying pH of the ionotropic solution components and  
39 by subsequent coating of the NPs with zein, increasing NP diameter to  $377\pm 47$ nm, whilst  
40 retaining polydispersity index and zeta potential values. Selenomethionine-entrapped  
41 nanoparticles were not cytotoxic to intestinal and liver cell lines. Accelerated thermal  
42 stability studies indicated good stability of the nanoparticles under **normal storage conditions**  
43 **(23°C)**. In simulated gastrointestinal and intestinal fluid conditions, 60% cumulative release  
44 was obtained over 6 hours.

45

46

47

48

49

50 **Keywords:**

51 chitosan, zein, selenomethionine, nanoparticles, Box-Behnken design, oral delivery

52

## 53 **Abbreviations**

54 **BBD**, Box-Behnken design; **CL113**, PROTASAN™ UP; **Cs**, Chitosan; **DLS**, dynamic light  
55 scattering; **EE%**, Encapsulation efficiency; **GRAS**, Generally recognised as safe; **LDV**, laser  
56 doppler velocimetry; **MSC**, methylselenocysteine; **NP**, nanoparticle; **PDI**, Polydispersity; **pI**,  
57 Isoelectric point; **SeCys**, selenocysteine; **SeMet**, Selenomethionine; **TPP**, Tripolyphosphate;  
58 **ZP**, Zeta potential.

## 59 **1 INTRODUCTION**

60 Selenium is an essential micronutrient in human and animal nutrition (Rayman, 2000), that  
61 exists in a wide array of different formats, both organic and inorganic, better known as  
62 speciation. Selenomethionine (SeMet), the selenium analogue of methionine, is the  
63 predominant form of organic Se found in foods from the *Brassica* and *Allium* families (Reilly  
64 et al., 2014). SeMet is used for oral supplementation due to its capacity to be non-specifically  
65 incorporated into body proteins in place of methionine (Rayman et al., 2008). The potential  
66 health benefits of selenium are dependent on its chemical species, and several studies have  
67 suggested a possible role in cancer prevention (Nie et al., 2016), increased immunological  
68 status (Narayan et al., 2015) and increased fertility (Shanmugam et al., 2015). SeMet may  
69 also to have a number of benefits regarding oncology treatments due to its modulation of the  
70 therapeutic efficacy and selectivity of anticancer drugs (Evans et al., 2017), capacity to  
71 provide protection of normal tissues from the toxicities associated with chemotherapy and  
72 radiation treatments, in addition to enhancing their anti-tumour effects (Chintala et al., 2012;  
73 Mix et al., 2015; Panchuk et al., 2016). It may also have some potential in degenerative  
74 disease by decreasing oxidative stress of small molecule antioxidants used as a buffer for free

75 radicals in brain tissue (Reddy et al., 2017; Song et al., 2014). However, the oral delivery of  
76 SeMet can be challenging due to the distinctive electronegativity and atomic radius of the  
77 selenium atom (i.e. larger radius and lower electronegativity than sulphur,) that makes it  
78 easier for low valence state Se compounds to be more readily oxidised compared to their  
79 sulphur counter parts (Xu et al., 2013). SeMet is readily oxidised (Davies, 2016) and, even  
80 though it is less toxic than inorganic selenium (Se), it still has a low therapeutic index  
81 (Takahashi et al., 2017). Oral delivery formulations of SeMet therefore need to consider the  
82 balance between doses that exert beneficial effects and those which may potentially be toxic.

83

84 Inorganic Se species such as selenite ( $\text{SeO}_3^{2-}$ ) and elemental selenium ( $\text{Se}_0$ ), together with  
85 methylseleninic acid, have been formulated to nano-enabled delivery systems which  
86 exhibited improved bioactivity with reduced cytotoxicity *in vitro* (Foorotanfar et al., 2014;  
87 Loeschner et al., 2014; Zhang et al., 2008). Nanoparticles (NPs) can be more biologically  
88 active due to their enhanced surface area per mass compared with larger-sized particles of the  
89 same chemistry (Oberdörster et al., 2005). By using NPs as a drug delivery vehicle, it might  
90 be possible to enhance a range of characteristics for a given bioactive, including; increased  
91 protection and stability (Nair et al., 2010) and suitability to increase bioavailability by non-  
92 parenteral routes of administration including oral, pulmonary and topical applications  
93 (Helson, 2013).

94

95 The natural polymer chitosan (Cs) is a mucopolysaccharide, closely related to cellulose and  
96 obtained by deacetylation of the compound chitin, predominantly found in the exoskeletons  
97 of crustaceans (Nagpal et al., 2010). Cs has been used for the development and formulation of  
98 nanoparticles by ionotropic gelation due to its physicochemical and biological beneficial  
99 properties (Mohammed et al., 2017; H. Zhang et al., 2015). Benefits include improved

100 adherence to mucosal surfaces, increased drug residence time (Ryan et al., 2012), and  
101 protection of the bioactive drug from intestinal proteases (Amaro et al., 2015; Ryan et al.,  
102 2013). In acidic medium, Cs can be dissolved, due to protonation of the amine residues  
103 present in the polymer backbone. Ionotropic gelation allows for the formation of NPs from  
104 Cs via crosslinking with oppositely-charged electrolytes under mild conditions in which  
105 amino acids and peptides will remain reasonably stable (Chen et al., 2013; Janes et al., 2001;  
106 Wang et al., 2011).

107  
108 Zein a GRAS approved prolamine-rich protein derived from maize, has been used in the  
109 formulation and coating of peptide oral delivery systems (Y. Zhang et al., 2015), to increase  
110 encapsulation efficiency (Luo and Wang, 2014) and improve the control of gastric release of  
111 labile bioactives (Luo et al., 2010; Paliwal and Palakurthi, 2014). By exploiting the physical  
112 interactions between protein and polysaccharide (in this instance zein and Cs), it is possible  
113 to improve and broaden the physical and chemical stability properties of the NP delivery  
114 systems (Benshitrit et al., 2012). However, the formulation, characterisation and development  
115 of these multi-component systems can be more challenging than single component systems  
116 and as such, it is important to comprehensively optimise the formulation process. To the best  
117 of our knowledge, there are currently no reports which describe the formulation of biological  
118 Se species such as SeMet into a NP delivery system. The potential optimisation of this  
119 formulation could be significant, given that SeMet more effectively increases human and  
120 animal selenium levels and is less toxic than inorganic Se (Garousi, 2015).

121  
122 In situations where several variables may influence system properties, a useful technique to  
123 identify the relationships between a given response and independent variables (or factors) and  
124 optimise the system, is Response Surface Methodology (RSM) (Anderson and Whitcomb,

125 2005). RSM is a more efficient approach to experimentation than one factor at a time (OFAT)  
126 experiments since it: 1) reduces the number of experimental runs typically required to gather  
127 the same information as OFAT, thus reducing resource requirements, 2) is useful in detecting  
128 interdependencies of variables that would not be typically identified during OFAT  
129 experiments and 3) improves the prediction of a response through use of gathered  
130 information from a larger parameter space. One of the most commonly applied RSM designs  
131 for process optimisation with a minimal experimental requirement is the Box-Benhken design  
132 (BBD), an independent quadratic design in which factor combinations are considered at 3  
133 levels; the midpoints of edges of the process space and the centre (Traynor et al., 2013;  
134 Zolgharnein et al., 2013). After polynomial models for each of the different responses in a  
135 study have been completed, a desirability function may be constructed in order to estimate  
136 minima or maxima, provided such optima are within the design space (Bezerra et al., 2008).

137

138 In this study, SeMet was formulated into nanoparticles consisting of Cs and zein using  
139 ionotropic gelation. After evaluating the main variables which affect encapsulation  
140 efficiency, particle size and drug loading, a systematic approach (RSM) was used to optimise  
141 the formulation of nanoparticles suitable for oral delivery. A three-level, three-factor BBD  
142 was utilised to build polynomial models for the three responses and a desirability function  
143 was then constructed to optimise the system. Optimised SeMet NPs were prepared based on  
144 the predicted optimum levels of the independent variables of the factorial design. To ensure  
145 stability of the optimised formulation after lyophilisation, a cryoprotectant (trehalose) was  
146 also included (Danish et al., 2017a). The physicochemical properties, storage stability,  
147 cytotoxicity, and the release profile in a simulated intestinal buffer were assessed.

## 148 **2 MATERIALS AND METHODS**

149 **2.1 Materials**

150 The chitosan **ultrapure** PROTASAN™ UP (CL113, Mw=110-150kDa, DDA=85%,  
151 **Endotoxins ≤ 100 EU/gram, Heavy metals ≤ 40 ppm**) was purchased from NovaMatrix, FMC  
152 Corporations, Norway. DL-selenomethionine, D(+)-Trehalose dihydrate, and zein, of ≥99%  
153 purity, were obtained from ACROS Organics™, Fisher Scientific, Ireland. Ultra-pure water  
154 18mΩcm<sup>-1</sup> was obtained from a Millipore simplicity 185 model instrument, UK, and was  
155 used for all aqueous solution preparations throughout. Sodium Tripolyphosphate (TPP) of  
156 **technical grade (85%)**, and all other reagents, chemicals and solvents were of analytical grade  
157 from Sigma Aldrich, Ireland.

158 **2.2 Optimisation of nanoparticle formulation physicochemical properties**

159 A BBD was used to optimise the formulation and EE% of SeMet into the nanoparticle.  
160 **Selected target physicochemical properties for oral delivery for the NPs were particle size of**  
161 **approximately 300 nm, PDI < 0.5 and ZP > 30 mV (des Rieux et al., 2006)**. A three level,  
162 three factor BBD (Maleki Dizaj et al., 2015; Zhao et al., 2013) of 15 random order  
163 experiments was designed using Minitab™ 17 (Pennsylvania, USA). The 3 independent  
164 variables were, (X<sub>1</sub>) the pH of the Cs solvent - the isoelectric point (pI) of SeMet, (pH-pI)  
165 (X<sub>2</sub>), the load concentration of SeMet and (X<sub>3</sub>) the ratio of Cs:TPP, while (Y<sub>1</sub>) Particle size,  
166 (Y<sub>2</sub>) PDI, (Y<sub>3</sub>) ZP and (Y<sub>4</sub>) EE% were the dependent variables. The variable ranges (Table  
167 1) were based on an exploratory study.

168 Each dependant variable was independently assessed by linear regression using a 2<sup>nd</sup> degree  
169 polynomial model with 1<sup>st</sup> order interactions (Eq. 1).

171 
$$Y_i = b_0 + b_1X_1 + b_2X_2 + b_3X_3 + b_{12}X_1X_2 + b_{13}X_1X_3 + b_{23}X_2X_3 + b_{11}X_1^2 + b_{22}X_2^2 + b_{33}X_3^2 + \varepsilon$$
  
172 **(Eq. 1)**

173 where  $Y_i$  is the measure of the response associated with each factor level combination,  $b_0$  is  
 174 an intercept,  $b_1$ - $b_{33}$  are the regression coefficients,  $X_1$ - $X_3$  are the coded independent variables  
 175 and the  $X_iX_j$  and  $X_i^2$  ( $i,j = 1, 2, 3$ ) denote the interactive and quadratic terms, respectively. The  
 176 linear regression and the significance ( $p < 0.05$ ) test of independent variables and their  
 177 interactions was assessed by statistical software (Minitab™,17) to generate regression  
 178 models. Through bidirectional elimination (testing at each step for variables to be included or  
 179 excluded), non-significant terms were removed from the model in order to calculate  
 180 regression equations with significant terms only (Wang et al., 2013). Desirability functions  
 181 to optimise all responses were built the weighted geometric mean of individual desirabilities  
 182 presented in Table 1.

183

184 **Table 1: Variables and levels employed in the BBD with desirability function for**  
 185 **optimisation of nanoparticle formulation.**

Factor (Independent variables)	Levels used, (Actual coded)		
$X_1$ = pH of the Cs solvent – the pI of SeMet (pH- pI)	0.5	1.5	2.5
$X_2$ = SeMet concentration (mg/mL)	0.05	0.15	0.25
$X_3$ = ratio of Cs:TPP	4:1	6:1	8:1
<b>Dependent Variables</b>	<b>Composite desirability</b>		
$Y_1$ = Size (nm)	Target of 300nm		
$Y_2$ = PDI	Minimise		
$Y_3$ = ZP (mV)	Maximise		
$Y_4$ = Encapsulation efficiency (EE%)	Maximise		

186

187 Response surface plots, statistical testing of the linear models and identification of optimum  
 188 formulations *via* feasibility and grid searches was performed to study the optimal area  
 189 (Barrentine, 1999). Finally, repetitions (N=4) of the optimal point found were conducted  
 190 experimentally to validate the study.

### 191 **2.3 Preparation of SeMet loaded Cs:TPP nanoparticles**

192 SeMet-entrapped NPs were produced using a modified ionic gelation method (Calvo et al.,  
193 1997). Briefly, Cs was dissolved in buffered pH medium (3, 4 or 5 pH) at a concentration of  
194 3 mg/mL and filtered through a 0.22  $\mu\text{m}$  syringe filter (Millex Millipore, UK) to remove  
195 undissolved Cs. A known amount of SeMet was then added to the Cs solution prior to  
196 crosslinking to obtain a final load concentration 0.05, 0.150 or 0.250 mg/mL. TPP was added  
197 dropwise to the solution under stirring at 700 rpm and room temperature to yield final mass  
198 ratios of Cs:TPP NPs of 4:1, 6:1 and 8:1. All of these experimental parameters (pH,  
199 concentrations and ratios) were prepared according to the BBD design. The NP suspension  
200 was stirred at 700 rpm for 30 min at room temperature for further crosslinking. After  
201 stabilisation, NPs were then transferred to a 30 kDa molecular weight cut off (Vivaspin 20,  
202 Sartorius) centrifugal filter and isolated by centrifugation at 3000 rpm for 30 min. Filtered  
203 H<sub>2</sub>O (equivalent in volume to the recovered supernatant) was then added to the isolated NPs  
204 and sonicated at 35 % amplitude for 30 s with 5 s pulse intervals. Physicochemical properties  
205 of the NPs were then determined as per section 2.4, using a Malvern Zetasizer NanoZS  
206 (Worcestershire, UK) and the supernatant was retained for EE% determination as outlined in  
207 section 2.7. The optimised formulation has a mass ratio 6:1 (Cs:TPP), Cs media (pH 5), and a  
208 final SeMet load concentration of 0.15 mg/mL.

#### 209 **2.3.1 Increase of Ionisation/Protonation states of NP components during ionic gelation to** 210 **increase EE% - Formulation I**

211 After optimising the general physicochemical properties via BBD (section 2.2), the ionic  
212 gelation component preparation procedure was modified with the aim of increasing the EE %.  
213 Formulation I was produced as described in section 2.3 with one exception; SeMet and TPP  
214 were dissolved and diluted with NaOH (0.01 M) prior to crosslinking. The rationale for the  
215 pH adjustment was to induce higher electrostatic interactions (i.e. maximise the cationic

216 component of Cs and the anionic component of SeMet) between SeMet and Cs during the  
217 crosslinking process.

### 218 **2.3.2 Coating NPs with zein to increase EE%**

219 NPs were prepared as per formulation I (ratio 6:1 (Cs:TPP), Cs media (pH 3), TPP/SeMet  
220 NaOH solution (pH 11) and a final load concentration of 0.15 mg/mL), with the following  
221 modifications; after the NPs had stabilised, 8 mL of absolute EtOH were added dropwise to  
222 the formulation whilst the stirring speed of the solution was maintained at 700 rpm for 30 min  
223 at room temperature. Zein (10 mg/mL dissolved in 80 % EtOH and filtered) was added  
224 dropwise to yield zein:Cs mass ratios of 0.5:1, 1:1 and 2:1, stabilised at 700 rpm for 30 min  
225 and isolated as per section 2.3. The NP formulations were then concentrated under vacuum  
226 (175 mbar) at 40 °C until EtOH was completely removed. To ensure stability of the  
227 optimised formulation after lyophilisation, 10 mL of the cryoprotectant trehalose 5 % w/v in  
228 H<sub>2</sub>O was added to each formulation and lyophilised for 36 hr (Danish et al., 2017a).  
229

### 230 **2.4 Nanoparticle Characterisation: Particle size, PDI and surface charge**

231 Freshly prepared NP solutions were used for physicochemical analysis (Luo et al., 2010). The  
232 mean particle size and PDI of the NP formulations were determined by dynamic light  
233 scattering (DLS). The ZP values were measured with the use of laser doppler velocimetry  
234 (LDV). Both DLS and LDV analysis were performed in triplicate at 25 °C with a Zetasizer  
235 Nano series Nano-ZS ZEN3600 fitted with a 633 nm laser (Malvern Instruments Ltd., UK),  
236 using a folded capillary cuvette (Folded capillary cell-DTS1060, Malvern, UK). The values  
237 presented herein were acquired from three separate experiments, each of which included  
238 three replicates; N=3.

## 239 **2.5 Scanning electron microscopy (SEM)**

240 NP morphology was evaluated by scanning electron microscopy (SEM) (Hitachi, SU6600  
241 FESEM, USA), at an accelerating voltage of 20 kV, unless otherwise stated, using the  
242 secondary electron detector. The fresh NP solutions were then spin coated onto Si wafers,  
243 dried at room temperature and then sputter coated with 4 nm Au/Pd prior to imaging  
244 (Mukhopadhyay et al., 2013).

## 245 **2.6 Fourier transform infrared spectroscopy (FTIR)**

246 FTIR spectra of CL113, TPP, Cs:TPP NPs, SeMet and SeMet loaded Cs:TPP NPs were  
247 acquired via a Spotlight 400 series spectrometer (Perkin Elmer, USA), using the attenuated  
248 total reflectance spectroscopy method (ATR-FTIR), in the range of 650-4000  $\text{cm}^{-1}$ . Prior to  
249 analysis, NP samples were lyophilised using a FreeZone 6 L bench top freeze dry system  
250 (Labconco, USA) at  $-40\text{ }^{\circ}\text{C}$  for 20 hr. The dried solids were then placed on the ATR crystal  
251 prism (ZnSe), and 32 scans were acquired at  $4\text{ cm}^{-1}$  resolution with background subtraction  
252 **using the empty sample holder** (Vongchan et al., 2011).

## 253 **2.7 EE% of SeMet in Cs:TPP nanoparticles**

254 The EE% of SeMet in the NPs was determined by the separation and quantification of SeMet  
255 left in the supernatant. This was performed by ultracentrifugation at 3000 rpm,  $4\text{ }^{\circ}\text{C}$  for 30  
256 min. SeMet in the supernatant was quantified by reverse phase high performance liquid  
257 chromatography (RP-HPLC), as previously described (Ward et al., 2012) with the following  
258 modifications. Samples were analysed with a Waters 2998 HPLC and Photodiode Array  
259 Detector, (Waters, USA), using a Poroshell 120, EC-C8 column,  $3.0 \times 100\text{ mm}$ ,  $2.7\text{ }\mu\text{m}$ ,  
260 (Agilent Technologies, UK). Isocratic elution was carried out at a flow rate of  $0.4\text{ mL/min}$ ,  
261 column temperature  $45.0 \pm 5.0\text{ }^{\circ}\text{C}$  with a mobile phase of water/methanol/trifluoroacetic acid

262 (97.9:2.0:0.1). Samples were monitored according to their UV absorbance at 218 nm. The  
263 encapsulation efficiency was calculated by Eq. 2 (Xu and Du, 2003);

264

$$265 \quad EE\% = \frac{\text{Total amount of Se Met} - \text{Free amount of SeMet}}{\text{Total amount of SeMet}} \times 100$$

266

(Eq. 2)

## 267 2.8 MTS assay

268 The potential cytotoxicity of pure SeMet, SeMet loaded NPs and unloaded NPs (coated with  
269 zein) were examined on Caco-2 human epithelial cells, and HepG2 human liver  
270 hepatocellular cells. Both cell lines are routinely employed to assess the potential toxicity of  
271 orally delivered compounds (Brayden et al., 2015; Gleeson et al., 2015). Caco-2 and HepG2  
272 cells, were seeded at a density of  $2 \times 10^4$  cells/well and cultured on 96 well plates in  
273 Dulbecco's Modified Eagle Medium (DMEM) and Eagle's Minimum Essential Medium  
274 (EMEM) respectively, supplemented with 10 % foetal bovine serum, 1 % L-glutamine, 1 %  
275 penicillin-streptomycin and 1 % non-essential amino acids at 37 °C in a humidified incubator  
276 with 5 % CO<sub>2</sub> and 95 % O<sub>2</sub>. Time points were selected with the intention to mimic *in vivo*  
277 conditions for each cell type. As the maximum time NPs will be exposed to the intestine, a 4  
278 hr exposure time was used in Caco-2 cell lines (Neves et al., 2016), to mimic the liver, a 72-  
279 h exposure time was used for HepG2 cell lines (Brayden et al., 2014). Triton X-100™  
280 (0.05%) was used as a positive control. The concentrations of the test compounds applied  
281 were 25, 50 and 100 μM. After exposure, treatments were removed and replaced with MTS  
282 (3-(4,5-dimethylthiazol-2-yl)-5-(3-carboxymethoxyphenyl)-2-(4-sulfophenyl)-2H-  
283 tetrazolium). Optical density (OD) was measured at 490 nm using a microplate reader  
284 (TECAN GENios, Grodig, Austria). Each value presented was normalised against untreated  
285 control and calculated from three separate experiments, each of which included six replicates.

## 286 **2.9 Accelerated stability analysis**

287 NPs were suspended at a concentration of 0.1 mg/mL, in aqueous KCl solution (10 mM) and  
288 stored at accelerated conditions; 60 °C for 720 min, 70 °C for 300 min and 80 °C for 120 min  
289 (Danish et al., 2017b). The particle size, PDI and ZP were measured using the Nanosizer ZS  
290 (Malvern Instruments Ltd, UK) over time intervals to determine the degree of degradation.  
291 The generated data was then analysed via R software (R Core Team, 2016). The temperature  
292 dependence of the kinetic parameters of SeMet-loaded NPs stability was measured by  
293 calculating the observed rate constants. This was plotted in an Arrhenius representation and  
294 apparent activation energy,  $E_a$  and reaction rate constant,  $k_{ref}$  were calculated according to Eq.  
295 3;

$$P = P_0 + e^{\ln(k) - \frac{E_a}{R} \left( \frac{1}{T} - \frac{1}{T_{ref}} \right)} t$$

296 (Eq.3)

297 where P is the property (particle size, PDI or ZP) at time t,  $P_0$  is the initial property  
298 conditions, k is the apparent zero order reaction constant,  $E_a$  is the energy of activation, R is  
299 the universal gas constant, T is the temperature of the experiment in Kelvin (K) and  $T_{ref}$  is the  
300 reference temperature (343 K).

## 301 **2.10 *In vitro* controlled release studies**

302 SeMet release from the NPs was carried out using a dialysis bag diffusion technique  
303 (Hosseinzadeh et al., 2012) over 6 hr (Calderon L. et al., 2013; Yoon et al., 2014). Freeze  
304 dried SeMet loaded NPs were suspended in 5 mL H<sub>2</sub>O and sonicated at 35 % amplitude for  
305 30 s with 5 s intervals and placed into a Float-A-Lyzer<sup>®</sup> G2 dialysis membrane with a pore  
306 size of 25 kDa (Spectrum Laboratories, USA). The sample was placed into 40 mL of  
307 simulated gastric fluid (SGF) or simulated intestinal fluid (SIF) specified according to the  
308 British Pharmacopoeia (Pharmacopoeia, 2016). SGF was composed of 0.1 M HCL and SIF

309 was composed of 1 volume of 0.2 M trisodium phosphate dodecahydrate and 3 volumes of  
310 0.1 M HCL (adjusted to pH 6.8), without enzymes (British Pharmacopoeia Commission,  
311 2016). Samples were placed in a thermostatic shaker at 37 °C and agitated at 100 rpm. At  
312 predetermined time points, 1 mL of release fluid was analysed and replaced with simulated  
313 fluid to maintain sink conditions.

314

315 SeMet release was measured by RP-HPLC (section 2.7). Eq. (4) was used to determine the %  
316 drug release;

317

$$Drug_{rel} \% = \frac{C(t)}{C(l)} * 100$$

318

(Eq. 4)

319 where  $Drug_{rel}$  is the percentage of SeMet released,  $C(l)$  represents the concentration of drug  
320 loaded and  $C(t)$  represents the amount of drug released at time t, respectively.

321

## 322 **3 RESULTS AND DISCUSSION**

### 323 **3.1 Response Surface Modelling – Box Behnken design**

324 The observed values for all 15 experiments described by the BBD yielded minimum and  
325 maximum values for Size ( $Y_1$ ) (152, 318 nm), PDI ( $Y_2$ ) (0.218, 0.554), ZP ( $Y_3$ ) (26.0, 42.7  
326 mV) and EE% ( $Y_4$ ) of, (24.7, 41.4 %). The reduced models resulting from the analysis are  
327 presented in table 2. Response  $Y_1$  showed no significant terms in the model, suggesting that  
328 there was no evidence in the sample population that could prove the association of the  
329 independent variables with particle size. This finding is unsurprising, as the NPs produced in  
330 this study fell within a narrow target region (152, 318 nm) and the regions of interest chosen

331 in this study (e.g. Cs:TPP 4:1-8:1, pH 3-5), to produce the Cs NPs, have been well  
332 established for yielding particle sizes within 100-400 nm range (Hassani et al., 2015;  
333 Mohammed et al., 2017; Sipoli et al., 2015).

334

335 Responses  $Y_2$ - $Y_4$  (PDI, ZP and EE% respectively) all showed a curvature with regards to  $X_1$ -  
336  $X_3$ , as quadratic or interactive effects of some independent variables were statistically  
337 significant in all the models.

338

339 **Table 2: Coded variable estimated coefficients (Coef) with associated standard error (SE Coef.)**  
 340 **and uncoded reduced regression equations for  $Y_2$ - $Y_4$ .**

Y <sub>2</sub> (PDI)			Y <sub>3</sub> (ZP)			Y <sub>4</sub> (EE%)		
Term	Coef	SE Coef	Term	Coef	SE Coef	Term	Coef	SE Coef
Constant	0.30833	0.00630	Constant	35.534	0.293	Constant	31.731	0.814
X <sub>1</sub> (pH-pI)	0.05150	0.00386	X <sub>1</sub> (pH-pI)	6.405	0.300	X <sub>1</sub> (pH-pI)	6.113	0.599
X <sub>2</sub> (SeMet (mg/mL))	0.00838	0.00386	X <sub>2</sub> (SeMet (mg/mL))	-	-	X <sub>2</sub> (SeMet (mg/mL))	-	-
X <sub>3</sub> (Ratio of Cs:TPP)	0.05213	0.00386	X <sub>3</sub> (Ratio of Cs:TPP)	1.245	0.300	X <sub>3</sub> (Ratio of Cs:TPP)	0.487	0.599
X <sub>1</sub> *X <sub>1</sub>	-0.06129	0.00568	X <sub>1</sub> *X <sub>1</sub>	-	-	X <sub>1</sub> *X <sub>1</sub>	3.821	0.879
X <sub>2</sub> *X <sub>2</sub>	0.10396	0.00568	X <sub>2</sub> *X <sub>2</sub>	-	-	X <sub>2</sub> *X <sub>2</sub>	-	-
X <sub>3</sub> *X <sub>3</sub>	0.06446	0.00568	X <sub>3</sub> *X <sub>3</sub>	-2.626	0.419	X <sub>3</sub> *X <sub>3</sub>	-3.529	0.879
X <sub>1</sub> *X <sub>2</sub>	-0.01750	0.00545	X <sub>1</sub> *X <sub>2</sub>	-	-	X <sub>1</sub> *X <sub>2</sub>	-	-
X <sub>1</sub> *X <sub>3</sub>	0.01650	0.00545	X <sub>1</sub> *X <sub>3</sub>	-	-	X <sub>1</sub> *X <sub>3</sub>	-	-
X <sub>2</sub> *X <sub>3</sub>	-0.04025	0.00545	X <sub>2</sub> *X <sub>3</sub>	-	-	X <sub>2</sub> *X <sub>3</sub>	-	-
<b>Lack of fit</b>	<b>0.27</b>		<b>Lack of fit</b>	<b>0.09</b>		<b>Lack of fit</b>	<b>0.62</b>	
<b>R<sup>2</sup>adjusted</b>	<b>98.66%</b>		<b>R<sup>2</sup>adjusted</b>	<b>98.65%</b>		<b>R<sup>2</sup>adjusted</b>	<b>90.82%</b>	
<b>Eq. (5)</b>	$Y_2 = 0.592 + 0.212 X_1 - 1.565 X_2 - 0.1495 X_3 - 0.06 X_1^2 X_1 + 10.40 X_2^2 X_2 + 0.01611 X_3^2 X_3 - 0.175 X_1 X_2 + 0.00825 X_1 X_3 - 0.2012 X_2 X_3$		<b>Eq. (6)</b>	$Y_3 = -1.21 + 6.405 X_1 + 8.49 X_3 - 0.6588 X_3^2 X_3$		<b>Eq. (7)</b>	$Y_4 = -2.06 + 5.35 X_1 + 10.83 X_3 + 3.821 X_1 X_1 - 0.882 X_3^2 X_3$	

341  
 342 In table 2 (Eq. 5), PDI was mostly affected by the quadratic effects of  $X_2^2 X_2$ , which showed  
 343 a positive correlation such that, at -1 and +1 levels of  $X_2$ , the PDI increased. It is also worth  
 344 noting that the linear term of  $X_2$  showed a negative coefficient, indicating that  $X_2$  has a  
 345 negative effect on PDI until a turning point is reached, whereafter  $X_2^2 X_2$  has a positive  
 346 impact on PDI. Similar findings were reported by Masarudin *et al.*, (2015), who found that  
 347 ratios of Cs:TPP less than 3:1 and greater than 12:1, resulted in a significant increase of the  
 348 formed NPs PDI values (>0.75). Additionally, they found that the NPs produced at ratios  
 349 between (median levels) the aforementioned upper and lower bounds resulted in NPs with PDI  
 350 values ranging from 0.15-0.32. A contour plot based on the regression model is presented in  
 351 Figure 1(A) and highlights this, showing that, at medium load concentrations of 0.15 mg/mL  
 352 and medium/low ratios of Cs:TPP (4.75:1 to 5.5:1), a minimum value for PDI can be  
 353 achieved. Conversely, as the concentration of TPP passes median levels PDI increases, which  
 354 may be attributable to TPP inducing cross-linking between the nanoparticles and thus the

355 presence of smaller aggregates within the solution (Antoniou et al., 2015a; Hu et al., 2008).  
356 Furthermore, the reduction of PDI as the concentration of TPP approaches median levels, has  
357 been shown to relate with the increased availability of TPP molecules to interact with the free  
358 amino groups of chitosan, thus allowing for additional incorporation of the anion within the  
359 nanoparticle chitosan chains (Huang and Lapitsky, 2017). Although PDI can be minimised at  
360 these particular levels, it is worth noting that the PDI values for all formulations fell within  
361 optimum values for oral delivery (Wong et al., 2017).

362

363 The results presented in table 2 (Eq.6) show that ZP was not affected by  $X_2$ , although it was  
364 affected by  $X_1$  (pH-pI) and  $X_3$  (Cs:TPP), indicating that the pH of the formulation medium  
365 and the electrostatic forces between the ionizable groups of Cs and TPP determine the net  
366 charge of the produced particles. It is likely that this is a direct consequence of the binding  
367 between the anionic phosphate groups of TPP with the positively charged amino acid  
368 moieties of Cs (Rampino et al., 2013), for example, a positive correlation was observed, such  
369 that ZP increased with increasing ratios. In addition,  $X_1$  also showed a prominent effect on  
370 ZP, whereby an increase in ZP is observed as  $X_1$  increases. The contour plot representing the  
371 reduced regression model (Figure 1(B)), demonstrates that low  $X_1$  levels (pH 5 - 4.2) and low  
372 ratios of Cs:TPP (4.0/4.5:1) are the areas where NPs of ZP <30mV were obtained (with a  
373 minimum of 27 mV). As  $X_1$  increases (approximately pH 3.5), an increment in ZP was  
374 observed and maximum values of >39 mV are achieved between  $X_3$  (ratio) of 4.5:1 - 7.5:1.  
375 This is in agreement with previous studies by Antoniou *et al.*, (2015), that showed at Cs: TPP  
376 mass ratios of 7:1, the ZP of the produced NPs decreased almost linearly with increasing pH  
377 of the formulation medium. As it has been shown that high ZP (either negative or positive),  
378 requires higher energy for bringing two particles in contact with each other (Dora et al.,  
379 2010), this pH-responsive behaviour can be attributed to the protonation of the primary amino

380 groups present on the Cs chain, resulting in an increase of electron density and repulsion  
381 forces between the crosslinked Cs chains (Lai and Guo, 2011). For example, at pH 3.5, the  
382 charge interaction between these two molecules becomes strong enough, and stable Cs NPs  
383 are obtained. On the contrary, at pH approaching the pI of Cs, reduced availability of  
384 protonated amine residues ( $-\text{NH}_3^+$ ) present on the Cs polymer backbone chain results in a  
385 lower surface charge of the formed NPs (Huang et al., 2015).

386

387 EE% was not affected by load concentration ( $X_2$ ) but was mostly affected by the pH of the Cs  
388 media (pH-pI ( $X_1$ )) (table 2 (Eq.7)), demonstrating the notable effect of SeMet loading with  
389 the charge of both polyelectrolytes (Cs and TPP) and their subsequent interaction during the  
390 crosslinking process. As can be seen, a negative correlation was observed, indicating that, as  
391  $X_1$  increases, the EE% decreases, most likely attributable to the reduced protonation of the  
392 primary amines present on Cs (Umerska et al., 2014). It is also worth noting that the  
393 quadratic term  $X_1 * X_1$  showed a positive coefficient, indicating  $X_1$  had a negative effect on  
394 EE% until a turning point was reached, where after  $X_1$  had a positive impact on EE%. He *et*  
395 *al.*, (2017), reported that by exploiting the ionic nature of insulin through modulation of the  
396 formulation media, the EE% of insulin into Cs:TPP NPs could be significantly enhanced,  
397 going from 37 to 94 %. This is evident in the contour plot produced by the regression model  
398 (Figure 1(C)) showing that, at maximum  $X_1$  levels (approximately 2.5 unit distance from pI  
399 of SeMet) and minimum to median/high ratios of Cs:TPP (4:1 - 7.5:1), maximum EE % (>40  
400 %) can be achieved, indicating that pH plays a significant role in the EE%. These findings  
401 agree with those of other research groups (Antoniou et al., 2015b; Janes et al., 2001), that  
402 reported a strategy to increase ionisable proteins (such as bovine serum albumin (BSA) and  
403 insulin) EE% (>80%) within a Cs NP matrix, by dissolving the load protein at a pH above its  
404 isoelectric point. By doing this, deprotonation of the hydroxy groups present on the load

405 cargo occurs, inducing a predominantly negative state and thus has a higher affinity to Cs and  
406 increased EE%. Several other studies have mirrored these findings, showing that the  
407 electrostatic interactions between the acidic groups present on insulin and the amino groups  
408 of Cs play a role in the association of insulin to the Cs-NPs by mediation of the ionic  
409 interaction between both macromolecules (Mattu et al., 2013; Pan et al., 2002).

410

411 **Figure 1: Contour Plot of (A) PDI against ratio of Cs:TPP ( $X_3$ ) and SeMet (mg/mL)**  
412 **( $X_2$ ), with pH-pI ( $X_1$ ) held at median level (1.5), (B) ZP against pH-pI ( $X_1$ ) and the ratio**  
413 **of Cs:TPP ( $X_3$ ) and (C) EE% against pH-pI ( $X_1$ ) vs ratio of Cs:TPP ( $X_3$ ) for the RSM**  
414 **models presented in Table 2.**

### 415 3.2 Optimisation

416 Employing the models constructed with the BBD evaluation in Table 2, response  
417 optimisation was employed in order to establish a formulation strategy to yield NPs with  
418 minimum PDI values, ZP of  $\geq 30$  mV and maximum EE% (des Rieux et al., 2006). As the  
419 range of NP sizes within all experimental runs fell within recommended target values for oral  
420 delivery, this response was excluded from the optimisation analysis.

421

422 Figure 2 shows the optimisation plot of the desired responses and indicates that, when the  
423 variable settings of  $X_1$ ,  $X_2$  and  $X_3$  are fixed at 2.5 (pH-pI), 0.15 (mg/mL) and 6 (Cs:TPP),  
424 respectively, NPs with the desired properties can be produced. Additionally, the 95 %  
425 confidence interval ranges of the predicted NP properties that these conditions would produce  
426 are presented in Table 3.

427

428 **Figure 2: Desirability profiles for optimisation of the formulation parameters;  $X_1$  (pH-**  
429 **pI),  $X_2$  (load concentration) and  $X_3$  (Ratio of Cs:TPP) - maximising ZP and EE%,**  
430 **whilst minimising PDI.**

431 **Table 3: 95% confidence interval for particle characteristics that optimal conditions**  
 432 **would produce under the present experimental conditions of uncertainty**

Response	Fit	95 % CI	Actual values
Y <sub>2</sub> (PDI)	0.299 ± 0.007	(0.282, 0.317)	0.284 ± 0.044
Y <sub>3</sub> (mV)	42.2 ± 2.0	(41.6, 42.7)	39.7 ± 2.6
Y <sub>4</sub> (EE%)	41.7 ± 1.0	(39.5, 43.8)	39 ± 3

433  
 434 To verify the validity of the proposed models, n = 4 replicates of the optimised formulation  
 435 were prepared, and each experimental response was compared with the predicted one. Table  
 436 3 shows the validation results of the model, whereby NPs presented sizes of 187 ± 58 nm,  
 437 PDI of 0.284 ± 0.044, ZP of 39.7 ± 2.6 mV and a max EE % of 39 ± 3 %. No statistical  
 438 significant values (p>0.05) for predicted and measured responses (Y<sub>2</sub>-Y<sub>4</sub>) were observed,  
 439 indicating that the models fit the data satisfactorily and has adequate precision for the  
 440 prediction of NP ZP, PDI and EE% in the chosen space of independent variables (in the  
 441 domain of levels chosen for the independent variables). Additionally, several consuming and  
 442 laborious laboratory studies were eliminated in this study by using the BBD, rather than a  
 443 OFAT approach.

### 444 **3.3 EE% optimisation I: protonation and ionisation**

445 The results from the BBD were promising in terms of the NPs produced and their  
 446 physicochemical properties. However, even when optimised, EE% remained low at  
 447 approximately 40 %. A second study was undertaken with the aim of maximising the EE%,  
 448 by controlling the ionisation process, given that this property primarily influenced the  
 449 encapsulation efficiency in the desirability profile (Figure 2). In the previous BBD, it was  
 450 noted that the highest EE% of SeMet within Cs:TPP NPs was obtained when the pH of the Cs  
 451 medium was maintained at pH 3 and the SeMet load was dissolved within it prior to  
 452 crosslinking. The fundamentals of ionotropic gelation exploit the opposing charges between

453 the protonated amine residues found on the glucosamine residue unit of Cs against the  
454 deprotonated hydroxyl groups on TPP (Janes et al., 2001). In order to increase the EE%, a  
455 modulation of the ionisation state of SeMet was achieved by dissolving it (and TPP) in a  
456 basic solution prior to crosslinking with Cs. The rationale for this approach is the observation  
457 that the pKa for the acid moiety of SeMet is pH 2.6, whereas the pKa for the basic moiety is  
458 at pH 8.9 (Foulkes, 2003) and as such, further electrostatic interactions can be induced at time  
459 of complexation (Qi et al., 2010). The effect of dissolving the TPP and SeMet in 0.01 M  
460 NaOH (pH 12) rather than H<sub>2</sub>O prior to crosslinking in the optimised formulation (ratio  
461 Cs:TPP 6:1, SeMet load concentration of 0.15 mg/mL and Cs medium pH of 3) was  
462 investigated, as a means to elicit greater interaction between Cs and SeMet and subsequently  
463 increase EE%. N= 3.

464

465 By altering the pH of the formulation, the EE% increased from  $39 \pm 3$  % to  $66 \pm 1$  %, whilst  
466 the physicochemical properties of the NPs remained within the target range for oral delivery  
467 (Table 4) (des Rieux *et al.*, 2006). This was most likely attributed to the electrostatic  
468 interactions between the now further ionised TPP and SeMet groups and protonated amine  
469 residues found on the glucosamine unit of Cs. This is consistent with the work by Pan et al.,  
470 (2014) which showed curcumin (CUR) successful encapsulation (>90%) into casein NPs,  
471 through deprotonation of CUR at pH 12, enabling for its re-association and thus subsequent  
472 encapsulation into the NP matrix.

473

474

### 475 **3.4 Improved Encapsulation Efficiency using zein**

476 The results from the first EE% optimisation study (Table 4) were promising, in terms of  
477 increasing EE% in addition to maintaining the desired NP physicochemical properties.

478 Nevertheless, the maximum EE% obtained by modifying the pH remained at  $66 \pm 4$  %.

479 Therefore, a subsequent step, involving the coating of the optimised NPs with zein (at  
480 varying zein:Cs mass ratios), was pursued as a means to increase the encapsulation efficiency  
481 of SeMet into the Cs: TPP NPs.

482

483 As shown in Table 4, as the ratio of zein in the formulation increased, the EE% improved. At  
484 0.5:1, zein:Cs, the average EE% achieved was 75 % and approximately 5 % increments in  
485 EE% were observed with subsequent increments of zein:Cs. The physicochemical properties  
486 of the NPs (PDI and ZP) were still within the target range for oral delivery for formulations  
487 with zein:Cs ratios  $\leq 1:1$ , although an increase in NP size was observed upon increasing zein  
488 concentrations. At a ratio of 2:1, zein:Cs, the physicochemical properties of the NPs were less  
489 than ideal, as large particle sizes (721 nm average) and high PDI values (0.783) were yielded,  
490 most likely as a consequence of a denser and thicker coating (Luo et al., 2010) provided by  
491 the partial deposition of the negatively charged protein on the particle surface, thus reducing  
492 the total net charge and inducing particle swelling (Rampino et al., 2013). For example, as the  
493 zein concentration increases, so does the viscosity of the dispersion, which can affect the  
494 nucleation process leading to the production of larger sized NPs (Zhong and Jin, 2009).

495 Similar results have been observed by others, whereby, an increase in zein concentration led  
496 to an increase in particle size of 6,7-dihydroxycoumarin loaded zein NPs (Podaralla and  
497 Perumal, 2012) or alpha-tocopherol loaded zein NPs, stabilised with Cs (Luo et al., 2012).

498 Lastly, the ZP of this formulation was the lowest observed (average of + 6 mV), which may  
499 be attributed to the increasing zein concentration, causing increased masking of the free  
500 positively charged amino groups of Cs (Krauland and Alonso, 2007). It is also possible that  
501 agglomeration occurred as a result of the reduced electrostatic repulsion between the NPs in  
502 suspension (Liu and Gao, 2009).

503

504 **Table 4: Physiochemical results for SeMet loaded NPs (Ratio 6:1, SeMet in NaOH (0.15**

505 **mg/mL load), Cs in pH 3) coated with zein. Size, PDI, ZP and EE% are presented for**

506 **each NP using different mass ratio combinations of zein and Cs. N=3.**

<b>Zein:Cs</b>	<b>Size (nm)</b>	<b>PDI</b>	<b>ZP (mV)</b>	<b>EE (%)</b>
<b>0:1</b>	<b>227 ± 17</b>	<b>0.448 ± 0.049</b>	<b>32 ± 1</b>	<b>66 ± 4</b>
<b>0.5:1</b>	<b>319 ± 19</b>	<b>0.221 ± 0.040</b>	<b>27 ± 6</b>	<b>74 ± 1</b>
<b>1:1</b>	<b>377 ± 47</b>	<b>0.325 ± 0.136</b>	<b>35 ± 6</b>	<b>81 ± 1</b>
<b>2:1</b>	<b>721 ± 108</b>	<b>0.783 ± 0.281</b>	<b>6 ± 4</b>	<b>85 ± 1</b>

507

508 **3.5 Characterisation of SeMet loaded and unloaded Cs:TPP NPs with and without**

509 **zein coating - Fourier transform infrared spectroscopy (FTIR)**

510 Figure 3 shows the FTIR spectra of (A) zein, (B) TPP, (C) Cs, (D) SeMet:Cs:TPP NPs and

511 (E) SeMet:Cs:TPP:zein NPs. The zein spectrum (Figure 3, A) shows characteristic peaks at

512 3289, 2929, 1644, 1515 and 1233  $\text{cm}^{-1}$  corresponding to; NH stretching vibrations, CH

513 stretching, amide I (C=O stretch), amide II (C-N and C-N-H/ in plane bending) and amide III

514 respectively (Podaralla and Perumal, 2012). Characteristic peaks for the phosphate ion (P=O)

515 in TPP (Figure 3, B) were observed at 1121  $\text{cm}^{-1}$  and 886  $\text{cm}^{-1}$ , respectively (Rampino et al.,

516 2013). Cs spectra (Figure 3, C) showed characteristic peaks at 3240, 2879, 1625, 1514, 1376

517 and 1063  $\text{cm}^{-1}$ . corresponding to NH Stretch / OH in pyranose ring, CH<sub>2</sub> in CH<sub>2</sub>OH group,

518 C=O in NHCOCH<sub>3</sub> group (amide I), NH<sub>2</sub> in NHCOCH<sub>3</sub> group (amide II), CH<sub>3</sub> in NHCOCH<sub>3</sub>

519 group and C-O-C (glycosidic linkage) respectively (Luo et al., 2010; Mohammed et al.,

520 2013).

521

522 **Figure 3: FTIR spectra of (A) zein, (B) TPP, (C) Cs, (D) SeMet:Cs:TPP NPs and (E)**

523 **SeMet:Cs:TPP:zein NPs. Spectra are offset for clarity.**

524

525 The FTIR spectrum of SeMet:Cs:TPP NPs (Figure 3, D) is different to that of the Cs matrix,  
526 as a result of intermolecular interactions of the constituent components. If interaction  
527 between the Cs and TPP had occurred, it will lead to frequency shifts or splitting in  
528 absorption peaks (Gan et al., 2005). For example, the peaks at  $1514\text{ cm}^{-1}$  in the Cs spectrum  
529 have been shifted to  $1560\text{ cm}^{-1}$ , indicating electrostatic interaction between the phosphate  
530 groups of TPP and the amino groups present in the Cs NP matrix (Papadimitriou et al., 2008).  
531 Additionally, the broadening and the increased absorbance of the peak at  $3272\text{ cm}^{-1}$  indicate  
532 hydrogen bonding has been enhanced (Luo et al., 2010). The band observed at  $1644\text{ cm}^{-1}$  in  
533 the zein FTIR spectrum (assigned to N-H bond), has been shifted to  $1648\text{ cm}^{-1}$  in the zein/Cs  
534 NPs spectrum (Figure 3, A and E respectively), indicating an interaction among the zein and  
535 Cs chains, possibly through hydrogen bonding among the amino groups present on both Cs  
536 and zein chains (Müller et al., 2011). Another indication of Cs:zein interaction arises from the  
537 amide III bands at  $1406\text{ cm}^{-1}$ , not visible in the zein spectrum, but now visible in the zein/Cs  
538 NPs (Figure 3, A and E respectively) spectrum, most likely as a result of the C-N stretching  
539 and out of plane N-H deformation being highly sensitive to structural changes (Sessa et al.,  
540 2008).

541

542 Lastly, the formation of zein/Cs NPs (E) is also characterised by the appearance of a band at  
543  $1041\text{ cm}^{-1}$  (assigned to C-O-C (glycosidic linkage)), which was observed in Cs/SeMet NPs  
544 (D) at  $1028\text{ cm}^{-1}$  but not observed in the zein spectrum (A), supporting the presence of Cs  
545 within the NP matrix (Figure 3) (Müller et al., 2011). The crosslinked Cs also showed a peak  
546 for P = O at  $1151\text{ cm}^{-1}$  (Bhumkar and Pokharkar, 2006), further indicating electrostatic  
547 interaction between Cs and TPP (Figure 3, E). No significant SeMet peaks in either  
548 Cs/TPP/SeMet or Cs/TPP/SeMet/zein NPs spectra were observed, most likely due to the fact,

549 that only 0.07 % of the dried formulation is contributed by SeMet and it is consequently  
550 masked by the other formulation components.

### 551 **3.6 Scanning electron microscopy**

552 Figure 4 shows the SEM images of uncoated and zein coated Se loaded NPs. The particle size  
553 of the NPs after spin coating was in good agreement with the DLS measurements taken on  
554 the freshly prepared NPs. Spherical, well distributed particles for both coated and uncoated  
555 SeMet loaded NPs were observed. However, it is interesting to note that the zein coated NPs  
556 displayed a smoother surface than that of the uncoated. This may be attributed to the use of  
557 the acetic acid buffer used during the formulation process, as similar results have been  
558 observed in spin-cast zein films prepared from an aqueous ethanol solvent compared to an  
559 acetic acid solution, indicating that a rough and hydrophilic surface was acquired for the  
560 former, whilst the zein film produced from an acetic acid solution appeared to be smooth,  
561 featureless and more hydrophobic (Shi et al., 2009; Y. Zhang et al., 2015).

562

563 **Figure 4: SEM image of (A) SeMet:Cs:TPP NPs and (B) SeMet:Cs:TPP NPs coated**  
564 **with zein**

### 565 **3.7 Accelerated stability analysis of SeMet-loaded NPs coated with zein**

566 The principle aim of accelerated stability testing is to provide reasonable assurance that a  
567 pharmaceutical or food consumable will remain at an acceptable level of quality throughout  
568 its timespan in the market place (Bajaj et al., 2012; Waterman and Adami, 2005). Real-time,  
569 retained sample, cyclic temperature and acceleration, are the four categories into which  
570 stability testing procedures fall (Bhagyashree et al., 2015). In the latter, the product is  
571 subjected to elevated temperatures and/or humidity well above ambient values, to determine  
572 the temperature at which product failure (i.e. degradation) will occur.

573

574 The Arrhenius equation, upon which the interpretation of accelerated stability testing is  
575 based, allows for the determination of the activation energy and consequently, the  
576 degradation rate of a product at lower temperatures (i.e. ambient, refrigerated etc.). In this  
577 instance, the data acquired can then be used to project the shelf life of the product in a much  
578 shorter time than that of real time assessments (Ali et al., 2013; Bhagyashree et al., 2015).  
579 This is a beneficial approach to stability testing, as it results in a greatly reduced product  
580 development schedule.

581 Figure 5 shows the kinetic behaviour of the NP properties; size (A), PDI (B) and ZP (C) at  
582 temperatures ranging from 60-80 °C. The stability of the NPs decreased with increasing  
583 temperature. Little change was detected for all properties at 60 °C, over the course of 720  
584 min, whereas a more pronounced increment in size and PDI and a decrease in ZP was  
585 observed at 70 °C after 300 min. At 80 °C, destabilisation of the NP complexes was evident  
586 across all properties, whereby size increased from approximately 300 nm to > 800 nm, PDI  
587 from approximately 0.2 to >0.9 and ZP reduced from approximately 32 mV to < 18 mV,  
588 indicating that aggregation of the NPs had occurred (Wu et al., 2011).

589

590 **Figure 5: (1) Particle size, (2) PDI and (3) ZP analysis of SeMet loaded NPs exposed to**  
591 **(a) 80 °C, (b) 70 °C and (c) 60 °C, over time periods of 120, 300 and 720 min,**  
592 **respectively. N=3**

593 The one-step nonlinear regression analysis of the kinetic experiments shows that particle size  
594 and PDI fit to a zero-order kinetic behaviour, with an Arrhenius dependence of  $\ln(k_{\text{ref}}@70$   
595  $^{\circ}\text{C}) = 1.66 \pm 9.44 \text{ min}^{-1}$  and  $E_a = 452.57 \pm 570.59 \text{ kJ/mol}$  for size, and a  $\ln(k_{\text{ref}}@70^{\circ}\text{C}) =$   
596  $0.029 \pm 0.014 \text{ min}^{-1}$ , and an  $E_a = 182.31 \pm 42.64 \text{ kJ/mol}$  for PDI respectively. In terms of ZP,

597 an apparent first order mechanism fits the data better than that of an apparent zero order  
598 model, with an Arrhenius dependence of  $\ln(k_{\text{ref}}@70\text{ °C}) = 0.038 \pm 0.010 \text{ min}^{-1}$  and  $E_a =$   
599  $205.71 \pm 25.65 \text{ kJ/mol}$ . Additionally, as can be seen in figure 6, a linear correlation is evident  
600 between  $1/T$  and  $\ln k$ , indicating that the formulations will be stable under normal storage  
601 conditions. This was expected, as previous reports have shown that zein coatings can increase  
602 the colloidal stability of iron phosphate NPs (Van Leeuwen et al., 2014) and, when stabilised  
603 with Cs, results in high thermal resistance of the NPs over prolonged periods of time (Luo et  
604 al., 2013).

605

606 **Figure 6: Arrhenius plots for the (A) ZP, (B) PDI and (C) size accelerated studies of**  
607 **SeMet loaded NPs. N=3.**

### 608 **3.8 Cytotoxicity assessment of SeMet-loaded NPs**

609 The potential cytotoxicity of SeMet in its native form and unloaded or SeMet loaded NPs  
610 coated with zein, at different test concentrations (25, 50 and 100  $\mu\text{M}$ ), were examined on  
611 Caco-2 human epithelial cells, and HepG2 human liver hepatocellular cells, using the MTS  
612 assay. As the NPs will become exposed to the intestinal epithelia following oral delivery  
613 (leading to its facilitated transport and uptake), time points were selected with the intention to  
614 mimic *in vivo* conditions for each cell type, to assess the potential cytotoxicity of the  
615 formulated NPs (Gleeson et al., 2015; Brayden et al., 2015). Caco-2 cells were exposed for  
616 4h (figure 7(A)) and HepG2 cells for 72h (figure 7(B)). In Caco-2 exposures, no cytotoxicity  
617 was observed for unloaded or SeMet loaded NPs, in comparison to the negative control,  
618 across all tested concentrations. For HepG2 exposures, no cytotoxicity was observed for  
619 unloaded or SeMet loaded NPs coated with zein. Additionally, the lower concentrations (25  
620 and 50  $\mu\text{M}$ ) of native SeMet showed no cytotoxicity to either cell line, whereas a reduction in

621 HepG2 cell viability (figure 7(B)) for native SeMet, at the 100  $\mu$ M test concentration, was  
622 observed (approx. 66% cell viability).

623

624 Similar results were observed by Takahashi, Suzuki and Ogra, 2017, whereby SeMet showed  
625 no significant change on the viability of Caco-2 cell lines, although it did show marginal  
626 toxicity to HepG2 cells at concentrations > 80  $\mu$ g/mL after prolonged exposure (48 hr). This  
627 finding is also in agreement with other works that showed SeMet toxicity occurred at  
628 concentrations  $\geq$ 40  $\mu$ M in various hepatoma cell lines (Kajander et al., 1991). It has  
629 previously been shown that Cs nanoparticles can enhance the delivery of inorganic Se  
630 compounds whilst reducing its toxicity (C. Zhang et al., 2015). In this work, SeMet loaded  
631 NPs elicited no significant reduction in viability of either cell line at equivalent concentration  
632 (100  $\mu$ M), indicating that, by encapsulating SeMet within the Cs NP matrix, the cytotoxic  
633 effects of pure SeMet, can be reduced.

634

635 **Figure 7:** Cytotoxicity assessment of  SeMet,  unloaded NPs with zein coating and  
636  SeMet loaded NPs with zein coating, exposed for (a) 4h in Caco-2 cell lines and (b) 72h  
637 in HepG2 cell line at SeMet equivalent concentrations (25  $\mu$ M, 50  $\mu$ M and 100  $\mu$ M). Triton<sup>TM</sup>  
638 X-100 (0.05%) was used as positive control and percentage (%) of MTS converted was  
639 compared to untreated control. 1-Way ANOVA with Dunnetts's post-test \*\*\* P< 0.001, \*\*  
640 P< 0.01, Each value presented was normalised against untreated control and calculated from  
641 three separate experiments, each of which included six replicates. N=3

642

643

### 644 3.9 *In vitro* release studies

645 *In vitro* techniques are advantageous for modelling potential interactions between NPs and  
646 the *in vivo* environment of the GI tract. Simulated gastric fluid and membrane analysis  
647 models enable assessment of *in vivo* environments without the use of human cell lines  
648 (Gamboa and Leong, 2013). Figure 8, shows the cumulative release profile of SeMet loaded  
649 NPs coated with zein, after subjection to 2 hr in an SGF environment (pH 1.2) representative  
650 of the stomach, followed by a compartmental change to SIF (pH 6.8), representative of the  
651 intestine, for 4 hr. As can be seen,  $25 \pm 1$  % of SeMet was released after 2 hr in SGF, followed  
652 by  $33 \pm 3$  % in SIF for 4 hr. No significant difference in the release profile of SeMet loaded  
653 NPs without zein coating was observed (data not shown). However, it was necessary to keep  
654 zein in the formulation due to the increase in EE ( $\geq 80$  %).

655

656 The target site of absorption of SeMet is the jejunum, in the small intestine. Therefore, it is  
657 important to withstand the acidic environment of the stomach. Three basic mechanisms that  
658 are typically applied to describe the release of drugs from polymeric particles, are  
659 swelling/erosion, diffusion, and degradation (Liechty et al., 2010). In this work, the total  
660 cumulative release of SeMet from the zein coated NPs, after 6 hr in simulated gastrointestinal  
661 tract environments, was 58 %, indicating that degradation of the NP was slow and thus the  
662 mechanism may be diffusion/relaxation oriented. As such, the release kinetics of SeMet NPs,  
663 under the SGF and SIF sequential controlled release experiments, were fitted using the  
664 following diffusive models derived from swellable systems (Siepmann and Peppas, 2011;  
665 Danish *et al.*, 2017a).

666

667

668

669 For the SGF:

670 
$$\frac{M_t}{M_\infty} = ks_1 * (\sqrt{time}) + ks_2 * time$$

671 (Eq.8)

672 where  $M_t$  is the diffused mass at a given time,  $M_\infty$  is the asymptotic diffused mass at infinite  
 673 time, and  $ks_1$  and  $ks_2$  are the diffusive and relaxation rate constants respectively.

674  
 675 For the SIF:

676

677 
$$\frac{M_t}{M_\infty} - \frac{M_{120}}{M_\infty} = ki_1 * (\sqrt{time - 120}) + ki_2 * (time - 120)$$

678 (Eq.9)

679 where  $M_{120}$  is the predicted diffused mass at the time of changing from SGF to SIF (120  
 680 min),  $ki_1$  and  $ki_2$  are diffusive and relaxation rate constants.

681

682 **Table 5: Swellable model parameters for kinetic release studies SeMet NPs.  $ks$**   
 683 **represents the stomach compartment and  $ki$  the intestinal compartment, divided into**  
 684 **diffusion and relaxation mechanisms ( $i_1$  and  $i_2$ ). All parameters listed where statistically**  
 685 **significant, \*\*\*P < 0.001; \*P < 0.05.**

Parameters	Estimate	Std. Error	t-value	Significance code
$Ks_2$	0.17082	0.04092	4.175	***
$Ki_1$	0.69145	0.33863	2.042	*
$Ki_2$	0.10817	0.02105	5.140	***
$R^2_{adj}$	0.984			

686

687 Table 5 presents the fitted values for the rate constants in SGF ( $ks$ ) and SIF ( $ki$ ) for SeMet  
 688 NPs, with  $ks_1$ , representing a diffusion mechanism and  $ks_2$  a relaxation mechanism (Eq. 8, 9).  
 689 In terms of the stomach compartment (SGF, pH 1.2), no statistically significant  $ks_1$  parameter  
 690 was found, indicating that the primary mechanism for release in the stomach was via

691 relaxation, i.e. slower release, approaching zero-order kinetics. After 2 hr subjected to the  
692 SGF environment, a compartmental change was employed to mimic the movement of the  
693 NPs to the intestinal environment (SIF, pH 6.8), whereupon a combination of diffusion ( $k_{i1}$ )  
694 and relaxation ( $k_{i2}$ ) mechanisms were observed ( $p < 0.05$ ). Overall, the model employed (Eq.  
695 8, 9) predicted the experimental data well, with an  $R^2_{adj} > 0.98$ . These results were expected,  
696 as polysaccharides generally undergo solvent penetration, swelling and chain  
697 disentanglement and relaxation, resulting in their ultimate dissolution (Fu and Kao, 2010).  
698 Additionally, this result is in agreement with previous studies, reporting a diffusion and zero  
699 order kinetic profile for IPP and LKP loaded CsNPs, coated with zein (Danish *et al.*, 2017a)  
700 and that of other researchers, who observed that zein proved to be a good coating for NPs,  
701 whereby, the stronger the interaction of the load material (in this instance phenolic  
702 monoterpenes) with that of the wall material (zein) was evidenced by its controlled release  
703 over time (da Rosa *et al.*, 2015).

704

705 **Figure 8: Release kinetics of SeMet NPs coated with zein after 2 hr in SGF (pH 1.2) and**  
706 **4 hr in SIF (pH 6.8).**

707

## 708 **4 CONCLUSION**

709 In this study, SeMet-loaded Cs NPs were produced via ionotropic gelation. BBD was used to  
710 identify optimum formulation variables that would result in NPs with physicochemical  
711 properties thought to be suitable for oral delivery. BBD highlighted the optimum conditions  
712 for NP production, although EE% remained relatively low. By varying the formulation media  
713 pH, increased electrostatic interaction between the crosslinking polyelectrolytes and drug  
714 were achieved, resulting in an increase in EE %. Coating the NPs at a 1:1 mass ratio of  
715 Cs:zein, resulted in NPs with a doubled EE accompanied by an increase in diameter. These

716 NPs were then characterised *via* FTIR analysis, which identified the presence of key  
717 functional groups of the native components and identifying shifts in the crosslinked matrixes.  
718 SEM analysis showed that spherical, well distributed particles were observed. MTS  
719 cytotoxicity studies showed no decrease in cellular viability in either Caco-2 or HepG2 cell  
720 after 4 and 72 hr exposures, respectively. Accelerated thermal stability of the loaded NPs  
721 indicated good stability under normal storage conditions. Lastly, after 6 hr exposure to  
722 simulated intestinal buffers, the release profile of the formulation showed that  $\leq 60\%$  of the  
723 drug had been released. These findings infer that encapsulation of SeMet into a NP delivery  
724 system comprising food-derived components reveals an oral administration approach for this  
725 molecule.

726

727 **Funding:**

728 This work was supported by Department of Agriculture, Food and Marine under FIRM (Food  
729 Institutional Research Measure). Project Ref: 13F510.

730

731 **Conflict of interest:**

732 All authors have approved the final manuscript, and the authors declare that they have no  
733 conflicts of interest to disclose.

734

735 **References:**

736 Ali, M.S., Alam, M.S., Alam, N., Anwer, T., Safhi, M.M.A., 2013. Accelerated stability  
737 testing of a clobetasol propionate-loaded nanoemulsion as per ICH guidelines. *Sci.*  
738 *Pharm.* 81, 1089–1100. <https://doi.org/10.3797/scipharm.1210-02>  
739 Amaro, M.I., Tewes, F., Gobbo, O., Tajber, L., Corrigan, O.I., Ehrhardt, C., Healy, A.M.,  
740 2015. Formulation, stability and pharmacokinetics of sugar-based salmon calcitonin-

741 loaded nanoporous/nanoparticulate microparticles (NPMPs) for inhalation. *Int. J. Pharm.*  
742 483, 6–18. <https://doi.org/10.1016/j.ijpharm.2015.02.003>

743 Anderson, M.J., Whitcomb, P.J., 2005. *RSM simplified: optimizing processes using response*  
744 *surface methods for design of experiments*. Productivity press.

745 Antoniou, J., Liu, F., Majeed, H., Qi, J., Yokoyama, W., Zhong, F., 2015a. Physicochemical  
746 and morphological properties of size-controlled chitosan-tripolyphosphate nanoparticles.  
747 *Colloids Surfaces A Physicochem. Eng. Asp.* 465, 137–146.  
748 <https://doi.org/10.1016/j.colsurfa.2014.10.040>

749 Antoniou, J., Liu, F., Majeed, H., Qi, J., Yokoyama, W., Zhong, F., 2015b. Physicochemical  
750 and morphological properties of size-controlled chitosan-tripolyphosphate  
751 nanoparticles. *Colloids Surfaces A Physicochem. Eng. Asp.* 465, 137–146.

752 Bajaj, S., Sakhuja, N., Singla, D., Bajaj Principal, S., 2012. Stability Testing of  
753 Pharmaceutical Products. *J. Appl. Pharm. Sci.* 02, 129–138.  
754 <https://doi.org/10.7324/JAPS.2012.2322>

755 Barrentine, L.B., 1999. *An introduction to design of experiments: a simplified approach*.  
756 ASQ Quality Press.

757 Benschitrit, R.C., Levi, C.S., Tal, S.L., Shimoni, E., Lesmes, U., 2012. Development of oral  
758 food-grade delivery systems: Current knowledge and future challenges. *Food Funct.* 3,  
759 10. <https://doi.org/10.1039/c1fo10068h>

760 Bezerra, M.A., Santelli, R.E., Oliveira, E.P., Villar, L.S., Escalera, L.A., 2008. Response  
761 surface methodology (RSM) as a tool for optimization in analytical chemistry. *Talanta*  
762 76, 965–77. <https://doi.org/10.1016/j.talanta.2008.05.019>

763 Bhagyashree, P., Karishma, G., Sampada, A., Ankita, P., Pratibha, C., Kailash, V., 2015.  
764 Recent trends in stability testing of pharmaceutical products: A review. *Res. J. Pharm.*  
765 *Biol. Chem. Sci.* 6, 1557–1569.

766 Bhumkar, D.R., Pokharkar, V.B., 2006. Studies on effect of pH on cross-linking of chitosan  
767 with sodium tripolyphosphate: a technical note. *Aaps Pharmscitech* 7, E138–E143.

768 Brayden, D.J., Cryan, S.-A., Dawson, K.A., O'Brien, P.J., Simpson, J.C., 2015. High-content  
769 analysis for drug delivery and nanoparticle applications. *Drug Discov. Today* 20, 942–  
770 957. <https://doi.org/10.1016/j.drudis.2015.04.001>

771 Brayden, D.J., Gleeson, J., Walsh, E.G., 2014. A head-to-head multi-parametric high content  
772 analysis of a series of medium chain fatty acid intestinal permeation enhancers in Caco-  
773 2 cells. *Eur. J. Pharm. Biopharm.* 88, 830–839.

774 British Pharmacopoeia Commission, 2016. *British Pharmacopoeia: Appendix XII B.*  
775 *Dissolution.* TSO, London.

776 Calderon L., Harris, R., Cordoba-Diaz, M., Elorza, M., Elorza, B., Lenoir, J., Adriaens, E.,  
777 Remon, J.P., Heras, A., Cordoba-Diaz, D., 2013. Nano and microparticulate chitosan-  
778 based systems for antiviral topical delivery. *Eur. J. Pharm. Sci.* 48, 216–222.  
779 <https://doi.org/10.1016/j.ejps.2012.11.002>

780 Calvo, P., Remunan ~~J.Lopez-Cos, V.M., Jato~~ 1997. Novel hydrophilic  
781 chitosan -polyethylene  
782 125–132.

783 Chen, M.C., Mi, F.L., Liao, Z.X., Hsiao, C.W., Sonaje, K., Chung, M.F., Hsu, L.W., Sung,  
784 H.W., 2013. Recent advances in chitosan-based nanoparticles for oral delivery of  
785 macromolecules. *Adv. Drug Deliv. Rev.* <https://doi.org/10.1016/j.addr.2012.10.010>

786 Chintala, S., Najrana, T., Toth, K., Cao, S., Durrani, F. a, Pili, R., Rustum, Y.M., 2012. Prolyl  
787 hydroxylase 2 dependent and Von-Hippel-Lindau independent degradation of Hypoxia-  
788 inducible factor 1 and 2 alpha by selenium in clear cell renal cell carcinoma leads to  
789 tumor growth inhibition. *BMC Cancer* 12, 293. [https://doi.org/10.1186/1471-2407-12-](https://doi.org/10.1186/1471-2407-12-293)  
790 293

791 da Rosa, C.G., de Oliveira Brisola Maciel, M.V., de Carvalho, S.M., de Melo, A.P.Z.,  
792 Jummes, B., da Silva, T., Martelli, S.M., Villetti, M.A., Bertoldi, F.C., Barreto, P.L.M.,  
793 2015. Characterization and evaluation of physicochemical and antimicrobial properties  
794 of zein nanoparticles loaded with phenolics monoterpenes. *Colloids Surfaces A*  
795 *Physicochem. Eng. Asp.* 481, 337–344. <https://doi.org/10.1016/j.colsurfa.2015.05.019>

796 Danish, M.K., Vozza, G., Byrne, H.J., Frias, J.M., Ryan, S.M., 2017a. Comparative study of  
797 the structural and physicochemical properties of two food derived antihypertensive tri-  
798 peptides, Isoleucine-Proline-Proline and Leucine-Lysine-Proline encapsulated into a  
799 chitosan based nanoparticle system. *Innov. Food Sci. Emerg. Technol.*  
800 <https://doi.org/10.1016/j.ifset.2017.07.002>

801 Danish, M.K., Vozza, G., Byrne, H.J., Frias, J.M., Ryan, S.M., 2017b. Formulation,  
802 Characterization and Stability Assessment of a Food-Derived Tripeptide, Leucine-  
803 Lysine-Proline Loaded Chitosan Nanoparticles. *J. Food Sci.* 82, 2094–2104.  
804 <https://doi.org/10.1111/1750-3841.13824>

805 Davies, M.J., 2016. Protein oxidation and peroxidation. *Biochem. J.* 473, 805–825.

806 des Rieux, A., Fievez, V., Garinot, M., Schneider, Y.-J., Pr at, V., 2006. Nanoparticles as  
807 potential oral delivery systems of proteins and vaccines: a mechanistic approach. *J.*  
808 *Control. release* 116, 1–27.

809 Dora, C.P., Singh, S.K., Kumar, S., Datusalia, A.K., Deep, A., 2010. Development and  
810 characterization of nanoparticles of glibenclamide by solvent displacement method. *Acta*  
811 *Pol. Pharm. - Drug Res.* 67, 283–290.

812 Evans, S.O., Khairuddin, P.F., Jameson, M.B., 2017. Optimising Selenium for Modulation of  
813 Cancer Treatments. *Anticancer Res.* 37, 6497–6509.

814 Forootanfar, H., Adeli-Sardou, M., Nikkhoo, M., Mehrabani, M., Amir-Heidari, B.,  
815 Shahverdi, A.R., Shakibaie, M., 2014. Antioxidant and cytotoxic effect of biologically

816 synthesized selenium nanoparticles in comparison to selenium dioxide. *J. Trace Elem.*  
817 *Med. Biol.* 28, 75–79.

818 Foulkes, M.E., 2003. Screening Methods for Semi-quantitative Speciation Analysis. *Handb.*  
819 *Elem. Speciat. Tech. Methodol.* 591.

820 Fu, Y., Kao, W.J., 2010. Drug Release Kinetics and Transport Mechanisms of Non-  
821 degradable and Degradable Polymeric Delivery Systems. *Expert Opin. Drug Deliv.* 7,  
822 429–444. <https://doi.org/10.1517/17425241003602259>

823 Gamboa, J.M., Leong, K.W., 2013. In vitro and in vivo models for the study of oral delivery  
824 of nanoparticles. *Adv. Drug Deliv. Rev.* 65, 800–810.  
825 <https://doi.org/10.1016/j.addr.2013.01.003>

826 Gan, Q., Wang, T., Cochrane, C., McCarron, P., 2005. Modulation of surface charge, particle  
827 size and morphological properties of chitosan–TPP nanoparticles intended for gene  
828 delivery. *Colloids Surfaces B Biointerfaces* 44, 65–73.

829 Garousi, F., 2015. The toxicity of different selenium forms and compounds – Review. *Acta*  
830 *Agrar. Debreceniensis* 64, 33–38.

831 Gleeson, J.P., Heade, J., Ryan, S.M.M., Brayden, D.J., 2015. Stability, toxicity and intestinal  
832 permeation enhancement of two food-derived antihypertensive tripeptides, Ile-Pro-Pro  
833 and Leu-Lys-Pro. *Peptides* 71, 1–7. <https://doi.org/10.1016/j.peptides.2015.05.009>

834 Hassani, S., Laouini, A., Fessi, H., Charcosset, C., 2015. Preparation of chitosan–TPP  
835 nanoparticles using microengineered membranes–Effect of parameters and  
836 encapsulation of tacrine. *Colloids Surfaces A Physicochem. Eng. Asp.* 482, 34–43.

837 He, Z., Santos, J.L., Tian, H., Huang, H., Hu, Y., Liu, L., Leong, K.W., Chen, Y., Mao, H.Q.,  
838 2017. Scalable fabrication of size-controlled chitosan nanoparticles for oral delivery of  
839 insulin. *Biomaterials* 130, 28–41. <https://doi.org/10.1016/j.biomaterials.2017.03.028>

840 Helson, L., 2013. Curcumin (diferuloylmethane) delivery methods: A review. *Biofactors* 39,

841 21–26.

842 Hosseinzadeh, H., Atyabi, F., Dinarvand, R., Ostad, S.N., 2012. Chitosan-Pluronic  
843 nanoparticles as oral delivery of anticancer gemcitabine: Preparation and in vitro study.  
844 *Int. J. Nanomedicine* 7, 1851–1863. <https://doi.org/10.2147/IJN.S26365>

845 Hu, B., Pan, C., Sun, Y., Hou, Z., Ye, H., Hu, B., Zeng, X., 2008. Optimization of fabrication  
846 parameters to produce chitosan– tripolyphosphate nanoparticles for delivery of tea  
847 catechins. *J. Agric. Food Chem.* 56, 7451–7458.

848 Huang, Y., Cai, Y., Lapitsky, Y., 2015. Factors affecting the stability of  
849 chitosan/tripolyphosphate micro- and nanogels: resolving the opposing findings. *J.*  
850 *Mater. Chem. B* 3, 5957–5970. <https://doi.org/10.1039/C5TB00431D>

851 Huang, Y., Lapitsky, Y., 2017. On the kinetics of chitosan/tripolyphosphate micro- and  
852 nanogel aggregation and their effects on particle polydispersity. *J. Colloid Interface Sci.*  
853 486, 27–37. <https://doi.org/10.1016/j.jcis.2016.09.050>

854 Janes, K.A., Calvo, P., Alonso, M.J., 2001. Polysaccharide colloidal particles as delivery  
855 systems for macromolecules. *Adv. Drug Deliv. Rev.* 47, 83–97.  
856 [https://doi.org/10.1016/S0169-409X\(00\)00123-X](https://doi.org/10.1016/S0169-409X(00)00123-X)

857 Kajander, E.O., Harvima, R.J., Eloranta, T.O., Martikainen, H., Kantola, M., Kärenlampi,  
858 S.O., Åkerman, K., 1991. Metabolism, cellular actions, and cytotoxicity of  
859 selenomethionine in cultured cells. *Biol. Trace Elem. Res.* 28, 57–68.  
860 <https://doi.org/10.1007/BF02990463>

861 Krauland, A.H., Alonso, M.J., 2007. Chitosan/cyclodextrin nanoparticles as macromolecular  
862 drug delivery system. *Int. J. Pharm.* 340, 134–142.

863 Lai, L.F., Guo, H.X., 2011. Preparation of new 5-fluorouracil-loaded zein nanoparticles for  
864 liver targeting. *Int. J. Pharm.* 404, 317–323.

865 Liechty, W.B., Kryscio, D.R., Slaughter, B. V, Peppas, N.A., 2010. Polymers for Drug

- 866 Delivery Systems. *Annu. Rev. Chem. Biomol. Eng.* 1, 149–173.  
867 <https://doi.org/10.1146/annurev-chembioeng-073009-100847>
- 868 Liu, H., Gao, C., 2009. Preparation and properties of ionically cross -linked chitosan  
869 nanoparticles. *Polym. Adv. Technol.* 20, 613–619.
- 870 Loeschner, K., Hadrup, N., Hansen, M., Pereira, S.A., Gammelgaard, B., Møller, L.H.,  
871 Mortensen, A., Lam, H.R., Larsen, E.H., 2014. Absorption, distribution, metabolism and  
872 excretion of selenium following oral administration of elemental selenium nanoparticles  
873 or selenite in rats. *Metallomics* 6, 330–337.
- 874 Luo, Y., Teng, Z., Wang, Q., 2012. Development of Zein Nanoparticles Coated with  
875 Carboxymethyl Chitosan for Encapsulation and Controlled Release of Vitamin D3. *J.*  
876 *Agric. Food Chem.* 60, 836–843. <https://doi.org/10.1021/jf204194z>
- 877 Luo, Y., Wang, Q., 2014. Zein-based micro- and nano-particles for drug and nutrient  
878 delivery: A review. *J. Appl. Polym. Sci.* 131, 1–12. <https://doi.org/10.1002/app.40696>
- 879 Luo, Y., Wang, T.T.Y., Teng, Z., Chen, P., Sun, J., Wang, Q., 2013. Encapsulation of indole-  
880 3-carbinol and 3,3'-diindolylmethane in zein/carboxymethyl chitosan nanoparticles with  
881 controlled release property and improved stability. *Food Chem.* 139, 224–230.  
882 <https://doi.org/10.1016/j.foodchem.2013.01.113>
- 883 Luo, Y., Zhang, B., Cheng, W.H., Wang, Q., 2010. Preparation, characterization and  
884 evaluation of selenite-loaded chitosan/TPP nanoparticles with or without zein coating.  
885 *Carbohydr. Polym.* 82, 942–951. <https://doi.org/10.1016/j.carbpol.2010.06.029>
- 886 Maleki Dizaj, S., Lotfipour, F., Barzegar-Jalali, M., Zarrintan, M.-H., Adibkia, K., 2015.  
887 Box-Behnken experimental design for preparation and optimization of ciprofloxacin  
888 hydrochloride-loaded CaCO<sub>3</sub> nanoparticles. *J. Drug Deliv. Sci. Technol.* 29, 125–131.  
889 <https://doi.org/10.1016/j.jddst.2015.06.015>
- 890 Masarudin, M.J., Cutts, S.M., Evison, B.J., Phillips, D.R., Pigram, P.J., 2015. Factors

891 determining the stability, size distribution, and cellular accumulation of small,  
892 monodisperse chitosan nanoparticles as candidate vectors for anticancer drug delivery:  
893 Application to the passive encapsulation of [14C]-doxorubicin. *Nanotechnol. Sci. Appl.*  
894 8, 67–80. <https://doi.org/10.2147/NSA.S91785>

895 Mattu, C., Li, R., Ciardelli, G., 2013. Chitosan nanoparticles as therapeutic protein  
896 nanocarriers: The effect of pH on particle formation and encapsulation efficiency.  
897 *Polym. Compos.* 34, 1538–1545.

898 Mix, M., Ramnath, N., Gomez, J., de Groot, C., Rajan, S., Dibaj, S., Tan, W., Rustum, Y.,  
899 Jameson, M.B., Singh, A.K., 2015. Effects of selenomethionine on acute toxicities from  
900 concurrent chemoradiation for inoperable stage III non-small cell lung cancer. *World J.*  
901 *Clin. Oncol.* 6, 156–165. <https://doi.org/10.5306/wjco.v6.i5.156>

902 Mohammed, M.A., Syeda, J.T.M., Wasan, K.M., Wasan, E.K., 2017. An overview of  
903 chitosan nanoparticles and its application in non-parenteral drug delivery. *Pharmaceutics*  
904 9. <https://doi.org/10.3390/pharmaceutics9040053>

905 Mohammed, M.H., Williams, P. a., Tverezovskaya, O., 2013. Extraction of chitin from prawn  
906 shells and conversion to low molecular mass chitosan. *Food Hydrocoll.* 31, 166–171.  
907 <https://doi.org/10.1016/j.foodhyd.2012.10.021>

908 Mukhopadhyay, P., Sarkar, K., Chakraborty, M., Bhattacharya, S., Mishra, R., Kundu, P.P.,  
909 2013. Oral insulin delivery by self-assembled chitosan nanoparticles: in vitro and in vivo  
910 studies in diabetic animal model. *Mater. Sci. Eng. C. Mater. Biol. Appl.* 33, 376–82.  
911 <https://doi.org/10.1016/j.msec.2012.09.001>

912 Müller, V., Piai, J.F., Fajardo, A.R., Fávoro, S.L., Rubira, A.F., Muniz, E.C., 2011.  
913 Preparation and characterization of zein and zein-chitosan microspheres with great  
914 prospective of application in controlled drug release. *J. Nanomater.* 2011, 10.

915 Nagpal, K., Singh, S.K., Mishra, D.N., 2010. Chitosan Nanoparticles: A Promising System in

916 Novel Drug Delivery. Chem. Pharm. Bull. (Tokyo). 58, 1423–1430.  
917 <https://doi.org/10.1248/cpb.58.1423>

918 Nair, H.B., Sung, B., Yadav, V.R., Kannappan, R., Chaturvedi, M.M., Aggarwal, B.B., 2010.  
919 Delivery of antiinflammatory nutraceuticals by nanoparticles for the prevention and  
920 treatment of cancer. Biochem. Pharmacol. 80, 1833–43.  
921 <https://doi.org/10.1016/j.bcp.2010.07.021>

922 Narayan, V., Ravindra, K.C., Liao, C., Kaushal, N., Carlson, B.A., Prabhu, K.S., 2015.  
923 Epigenetic regulation of inflammatory gene expression in macrophages by selenium. J.  
924 Nutr. Biochem. 26, 138–145.

925 Neves, A.R., Martins, S., Segundo, M.A., Reis, S., 2016. Nanoscale delivery of resveratrol  
926 towards enhancement of supplements and nutraceuticals. Nutrients 8, 131.

927 Nie, T., Wu, H., Wong, K.-H., Chen, T., 2016. Facile synthesis of highly uniform selenium  
928 nanoparticles using glucose as the reductant and surface decorator to induce cancer cell  
929 apoptosis. J. Mater. Chem. B 4, 2351–2358.

930 Oberdörster, G., Maynard, A., Donaldson, K., Castranova, V., Fitzpatrick, J., Ausman, K.,  
931 Carter, J., Karn, B., Kreyling, W., Lai, D., Olin, S., Monteiro-Riviere, N., Warheit, D.,  
932 Yang, H., 2005. Principles for characterizing the potential human health effects from  
933 exposure to nanomaterials: elements of a screening strategy. Part. Fibre Toxicol. 2, 8.  
934 <https://doi.org/10.1186/1743-8977-2-8>

935 Paliwal, R., Palakurthi, S., 2014. Zein in controlled drug delivery and tissue engineering. J.  
936 Control. Release 189, 108–22. <https://doi.org/10.1016/j.jconrel.2014.06.036>

937 Pan, Y., Li, Y.J., Zhao, H.Y., Zheng, J.M., Xu, H., Wei, G., Hao, J.S., Cui, F. De, 2002.  
938 Bioadhesive polysaccharide in protein delivery system: Chitosan nanoparticles improve  
939 the intestinal absorption of insulin in vivo. Int. J. Pharm. 249, 139–147.  
940 [https://doi.org/10.1016/S0378-5173\(02\)00486-6](https://doi.org/10.1016/S0378-5173(02)00486-6)

941 Panchuk, R.R., Skorokhyd, N.R., Kozak, Y.S., Lehka, L. V, Chumak, V. V, Omelyanchik,  
942 S.N., Gurinovich, V.A., Moiseenok, A.G., Stoika, R.S., 2016. Antioxidants  
943 selenomethionine and D-pantethine decrease the negative side effects of doxorubicin in  
944 NL/Ly lymphoma-bearing mice. *Croat. Med. J.* 57, 180–92.  
945 <https://doi.org/10.3325/cmj.2016.57.180>

946 Papadimitriou, S., Bikiaris, D., Avgoustakis, K., Karavas, E., Georgarakis, M., 2008.  
947 Chitosan nanoparticles loaded with dorzolamide and pramipexole. *Carbohydr. Polym.*  
948 73, 44–54.

949 Pharmacopoeia, B., 2016. British Pharmacopoeia Commission: London.

950 Podaralla, S., Perumal, O., 2012. Influence of formulation factors on the preparation of zein  
951 nanoparticles. *Aaps Pharmscitech* 13, 919–927.

952 Qi, J., Yao, P., He, F., Yu, C., Huang, C., 2010. Nanoparticles with dextran/chitosan shell and  
953 BSA/chitosan core-Doxorubicin loading and delivery. *Int. J. Pharm.* 393, 177–185.  
954 <https://doi.org/10.1016/j.ijpharm.2010.03.063>

955 Rampino, A., Borgogna, M., Blasi, P., Bellich, B., Cesàro, A., 2013. Chitosan nanoparticles:  
956 Preparation, size evolution and stability. *Int. J. Pharm.* 455, 219–228.  
957 <https://doi.org/https://doi.org/10.1016/j.ijpharm.2013.07.034>

958 Rayman, M.P., 2000. The importance of selenium to human health. *Lancet* 356, 233–241.  
959 [https://doi.org/10.1016/S0140-6736\(00\)02490-9](https://doi.org/10.1016/S0140-6736(00)02490-9)

960 Rayman, M.P., Infante, H.G., Sargent, M., 2008. Food-chain selenium and human health:  
961 spotlight on speciation. *Br. J. Nutr.* 100, 238–253.  
962 <https://doi.org/10.1017/S0007114508922522>

963 Reddy, V.S., Bukke, S., Dutt, N., Rana, P., Pandey, A.K., 2017. A systematic review and  
964 meta-analysis of the circulatory, erythrocellular and CSF selenium levels in Alzheimer’s  
965 disease: A metal meta-analysis (AMMA study-I). *J. Trace Elem. Med. Biol.* 42, 68–75.

966 Reilly, K., Valverde, J., Finn, L., Gaffney, M., Rai, D.K., Brunton, N., 2014. A note on the  
967 effectiveness of selenium supplementation of Irish-grown Allium crops. *Irish J. Agric.*  
968 *Food Res.* 91–99.

969 Ryan, K.B., Maher, S., Brayden, D.J., O’driscoll, C.M., 2012. .2: NANOSTRUCTURES  
970 OVERCOMING THE INTESTINAL BARRIER: DRUG DELIVERY STRATEGIES.  
971 Nanostructured Biomater. Overcoming Biol. Barriers 63.

972 Ryan, S.M., McMorrow, J., Umerska, A., Patel, H.B., Kornerup, K.N., Tajber, L., Murphy,  
973 E.P., Perretti, M., Corrigan, O.I., Brayden, D.J., 2013. An intra-articular salmon  
974 calcitonin-based nanocomplex reduces experimental inflammatory arthritis. *J. Control.*  
975 *Release* 167, 120–129.

976 Sessa, D.J., Mohamed, A., Byars, J.A., 2008. Chemistry and physical properties of melt-  
977 processed and solution-cross-linked corn zein. *J. Agric. Food Chem.* 56, 7067–7075.

978 Shanmugam, M., Prakash, B., REDDY, E.P.K., PANDA, A.K., 2015. Dietary organic zinc  
979 and selenium supplementation improves semen quality and fertility in layer breeders.  
980 *Indian J. Anim. Sci.* 85.

981 Shi, K., Kokini, J.L., Huang, Q., 2009. Engineering zein films with controlled surface  
982 morphology and hydrophilicity. *J. Agric. Food Chem.* 57, 2186–2192.  
983 <https://doi.org/10.1021/jf803559v>

984 Siepmann, J., Peppas, N.A., 2011. Higuchi equation: Derivation, applications, use and  
985 misuse. *Int. J. Pharm.* <https://doi.org/10.1016/j.ijpharm.2011.03.051>

986 Sipoli, C.C., Santana, N., Shimojo, A.A.M., Azzoni, A., de la Torre, L.G., 2015. Scalable  
987 production of highly concentrated chitosan/TPP nanoparticles in different pHs and  
988 evaluation of the in vitro transfection efficiency. *Biochem. Eng. J.* 94, 65–73.

989 Song, G., Zhang, Z., Wen, L., Chen, C., Shi, Q., Zhang, Y., Ni, J., Liu, Q., 2014.  
990 Selenomethionine ameliorates cognitive decline Song, G. et al. (2014)

991 'Selenomethionine ameliorates cognitive decline, reduces tau hyperphosphorylation, and  
992 reverses synaptic deficit in the triple transgenic mouse model of alzheimer's disease',  
993 Journal of . J. Alzheimer's Dis. 41, 85–99. <https://doi.org/10.3233/JAD-131805>

994 Takahashi, K., Suzuki, N., Ogra, Y., 2017. Bioavailability comparison of nine  
995 bioselenocompounds in vitro and in vivo. Int. J. Mol. Sci. 18, 1–11.  
996 <https://doi.org/10.3390/ijms18030506>

997 Traynor, M., Burke, R., Frias, J.M., Gaston, E., Barry-ryan, C., Traynor, M., Barry-ryan, C.,  
998 2013. Formation and Stability of an Oil in Water Emulsion Containing Lecithin ,  
999 Xanthan Gum and Sunflower Oil Formation and Stability of an Oil in Water Emulsion  
1000 Containing Lecithin , Xanthan Gum and Sunflower Oil 20, 2173–2181.

1001 Umerska, A., Corrigan, O.I., Tajber, L., 2014. Intermolecular interactions between salmon  
1002 calcitonin, hyaluronate, and chitosan and their impact on the process of formation and  
1003 properties of peptide-loaded nanoparticles. Int. J. Pharm. 477, 102–112.  
1004 <https://doi.org/10.1016/j.ijpharm.2014.10.023>

1005 Van Leeuwen, Y.M.M., Velikov, K.P.P., Kegel, W.K.K., 2014. Colloidal stability and  
1006 chemical reactivity of complex colloids containing Fe<sup>3+</sup>. Food Chem. 155, 161–166.  
1007 <https://doi.org/10.1016/j.foodchem.2014.01.045>

1008 Vongchan, P., Wutti-In, Y., Sajomsang, W., Gonil, P., Kothan, S., Linhardt, R.J., 2011. N, N,  
1009 N-Trimethyl chitosan nanoparticles for the delivery of monoclonal antibodies against  
1010 hepatocellular carcinoma cells. Carbohydr. Polym. 85, 215–220.

1011 Wang, J.J., Zeng, Z.W., Xiao, R.Z., Xie, T., Zhou, G.L., Zhan, X.R., Wang, S.L., 2011.  
1012 Recent advances of chitosan nanoparticles as drug carriers. Int. J. Nanomedicine.  
1013 <https://doi.org/10.2147/IJN.S17296>

1014 Wang, M., Wright, J., Buswell, R., Brownlee, A., 2013. A comparison of approaches to  
1015 stepwise regression for global sensitivity analysis used with evolutionary optimization,

1016 in: Proceedings of the BS2013, 13th Conference of International Building Performance  
1017 Simulation Association, Chambéry, France. pp. 26–28.

1018 Ward, P., Connolly, C., Murphy, R., 2012. Accelerated Determination of Selenomethionine  
1019 in Selenized Yeast: Validation of Analytical Method. *Biol. Trace Elem. Res.* 151, 446–  
1020 450. <https://doi.org/10.1007/s12011-012-9571-x>

1021 Waterman, K.C., Adami, R.C., 2005. Accelerated aging: prediction of chemical stability of  
1022 pharmaceuticals. *Int. J. Pharm.* 293, 101–125.

1023 Wong, C.Y., Al-Salami, H., Dass, C.R., 2017. The role of chitosan on oral delivery of  
1024 peptide-loaded nanoparticle formulation. *J. Drug Target.* 0, 1–12.  
1025 <https://doi.org/10.1080/1061186X.2017.1400552>

1026 Wu, L., Zhang, J., Watanabe, W., 2011. Physical and chemical stability of drug nanoparticles.  
1027 *Adv. Drug Deliv. Rev.* 63, 456–469.

1028 Xu, H., Cao, W., Zhang, X., 2013. Selenium-containing polymers: promising biomaterials for  
1029 controlled release and enzyme mimics. *Acc. Chem. Res.* 46, 1647–1658.

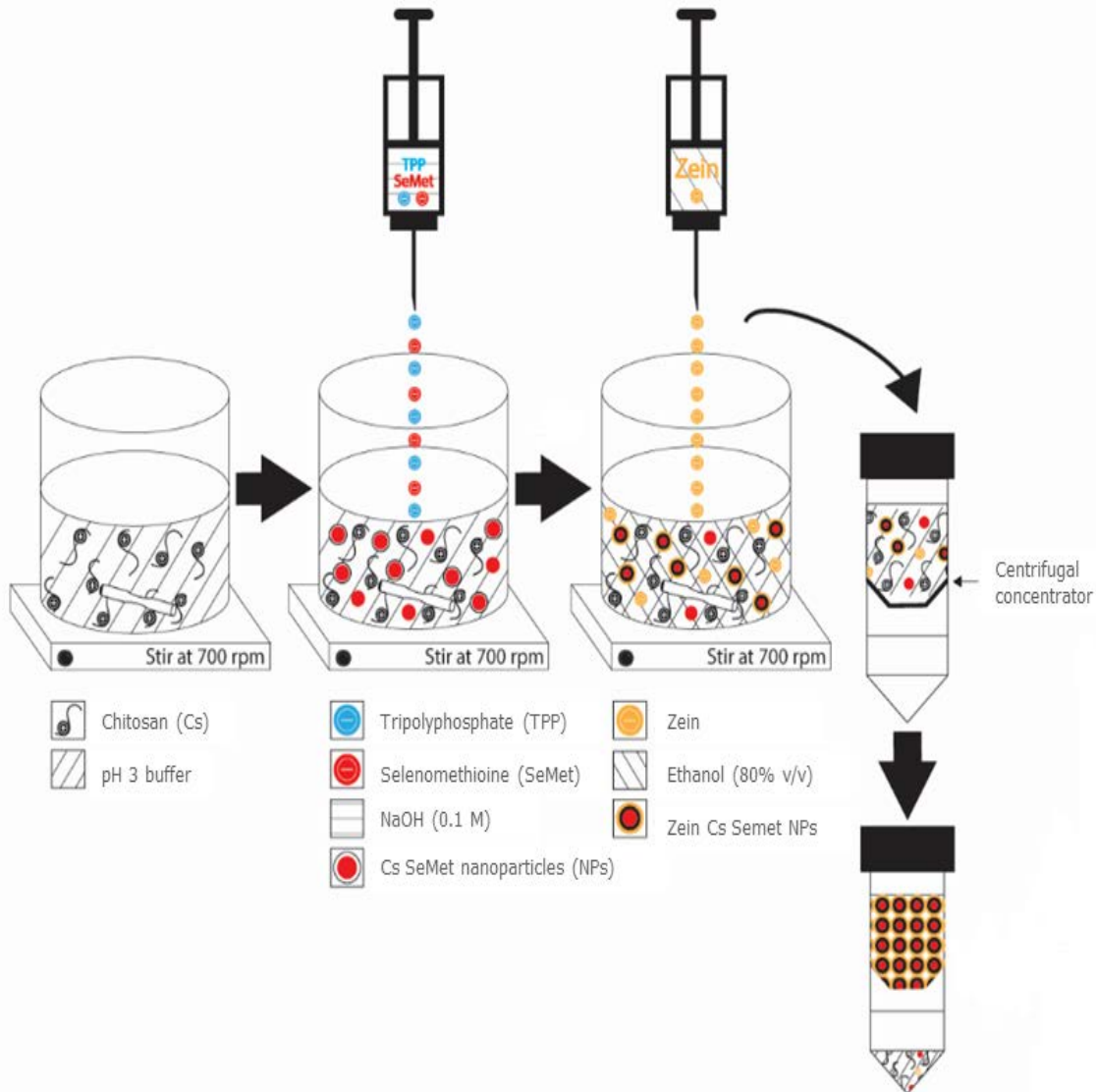
1030 Yoon, H.Y., Son, S., Lee, S.J., You, D.G., Yhee, J.Y., Park, J.H., Swierczewska, M., Lee, S.,  
1031 Kwon, I.C., Kim, S.H., Kim, K., Pomper, M.G., 2014. Glycol chitosan nanoparticles as  
1032 specialized cancer therapeutic vehicles: Sequential delivery of doxorubicin and Bcl-2  
1033 siRNA. *Sci. Rep.* 4, 6878. <https://doi.org/10.1038/srep06878>

1034 Zhang, C., Zhai, X., Zhao, G., Ren, F., Leng, X., 2015. Synthesis, characterization, and  
1035 controlled release of selenium nanoparticles stabilized by chitosan of different molecular  
1036 weights. *Carbohydr. Polym.* 134, 158–166.

1037 Zhang, H., Huang, Q., Huang, Z., Liu, T., Li, Y., 2015. Preparation and physicochemical  
1038 properties of chitosan broadleaf holly leaf nanoparticles. *Int. J. Pharm.* 479, 212–218.  
1039 <https://doi.org/10.1016/j.ijpharm.2014.12.010>

1040 Zhang, J., Wang, X., Xu, T., 2008. Elemental selenium at nano size (Nano-Se) as a potential

- 1041 chemopreventive agent with reduced risk of selenium toxicity: comparison with se-  
1042 methylselenocysteine in mice. *Toxicol. Sci.* 101, 22–31.
- 1043 Zhang, Y., Cui, L., Che, X., Zhang, H., Shi, N., Li, C., Chen, Y., Kong, W., 2015. Zein-based  
1044 films and their usage for controlled delivery: Origin, classes and current landscape. *J.*  
1045 *Control. Release* 206, 206–219. <https://doi.org/10.1016/j.jconrel.2015.03.030>
- 1046 Zhao, L., Zhu, B., Jia, Y., Hou, W., Su, C., 2013. Preparation of biocompatible  
1047 carboxymethyl chitosan nanoparticles for delivery of antibiotic drug. *Biomed Res. Int.*  
1048 2013, 1–8. <https://doi.org/10.1155/2013/236469>
- 1049 Zhong, Q., Jin, M., 2009. Zein nanoparticles produced by liquid–liquid dispersion. *Food*  
1050 *Hydrocoll.* 23, 2380–2387.
- 1051 Zolgharnein, J., Shahmoradi, A., Ghasemi, J.B., 2013. Comparative study of Box–Behnken,  
1052 central composite, and Doehlert matrix for multivariate optimization of Pb (II)  
1053 adsorption onto Robinia tree leaves. *J. Chemom.* 27, 12–20.
- 1054
- 1055 **Graphical abstract:**



1056

1057 The above graphic depicts the formulation methodology used to produce selenomethionine  
 1058 loaded chitosan nanoparticles, coated with zein, for *in vitro* assessment. Briefly, to produce  
 1059 the nanoparticles, chitosan was protonated by dissolving in acidic buffer (pH 3), then  
 1060 crosslinked with ionised tripolyphosphate and selenomethionine in NaOH (0.1 M). Zein  
 1061 coating was then employed to coat the nanoparticles and purification was achieved by  
 1062 removing unencapsulated formulation components through ultracentrifugation.

1063

1064 **Figure 1: Contour Plot of (A) PDI against ratio of Cs:TPP ( $X_3$ ) and SeMet (mg/mL)**  
 1065 **( $X_2$ ), with pH-pI ( $X_1$ ) held at median level (1.5), (B) ZP against pH-pI ( $X_1$ ) and the ratio**

1066 of Cs:TPP ( $X_3$ ) and (C) EE% against pH-pI ( $X_1$ ) vs ratio of Cs:TPP ( $X_3$ ) for the RSM  
1067 models presented in Table 2.

1068

1069 **Figure 2: Desirability profiles for optimisation of the formulation parameters;  $X_1$  (pH-  
1070 pI),  $X_2$  (load concentration) and  $X_3$  (Ratio of Cs:TPP) - maximising ZP and EE%,  
1071 whilst minimising PDI.**

1072

1073 **Figure 3: FTIR spectra of (A) zein, (B) TPP, (C) Cs, (D) SeMet:Cs:TPP NPs and (E)  
1074 SeMet:Cs:TPP:zein NPs. Spectra are offset for clarity.**

1075

1076 **Figure 4: SEM image of (A) SeMet:Cs:TPP NPs and (B) SeMet:Cs:TPP NPs coated  
1077 with zein**

1078

1079 **Figure 5: (1) Particle size, (2) PDI and (3) ZP analysis of SeMet loaded NPs exposed to  
1080 (a) 80 °C, (b) 70 °C and (c) 60 °C, over time periods of 120, 300 and 720 min,  
1081 respectively. N=3**

1082 **Figure 6: Arrhenius plots for the (A) ZP, (B) PDI and (C) size accelerated studies of  
1083 SeMet loaded NPs. N=3.**

1084

1085 **Figure 7: Cytotoxicity assessment of  SeMet,  unloaded NPs with zein coating and  
1086  SeMet loaded NPs with zein coating, exposed for (a) 4h in Caco-2 cell lines and (b) 72h  
1087 in HepG2 cell line at SeMet equivalent concentrations (25 uM, 50 uM and 100 uM). Triton™  
1088 X-100 (0.05%) was used as positive control and percentage (%) of MTS converted was  
1089 compared to untreated control. 1-Way ANOVA with Dunnetts's post-test \*\*\* P< 0.001, \*\*  
1090 P< 0.01, Each value presented was normalised against untreated control and calculated from  
1091 three separate experiments, each of which included six replicates. N=3**

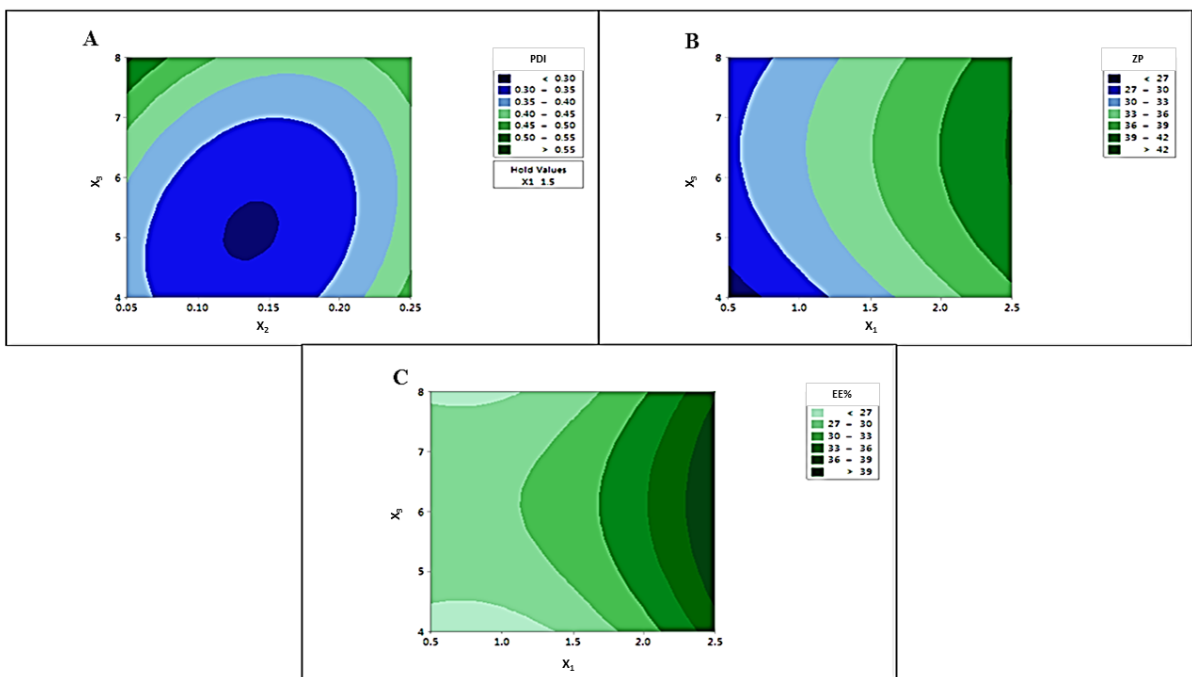
1092

1093 **Figure 8: Release kinetics of SeMet NPs coated with zein after 2 hr in SGF (pH 1.2) and**

1094 **4 hr in SIF (pH 6.8).**

1095

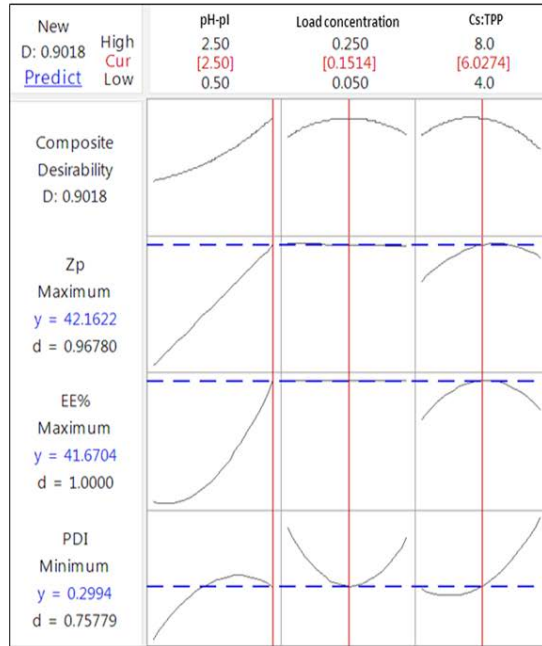
1096



1097

1098 **Figure 1**

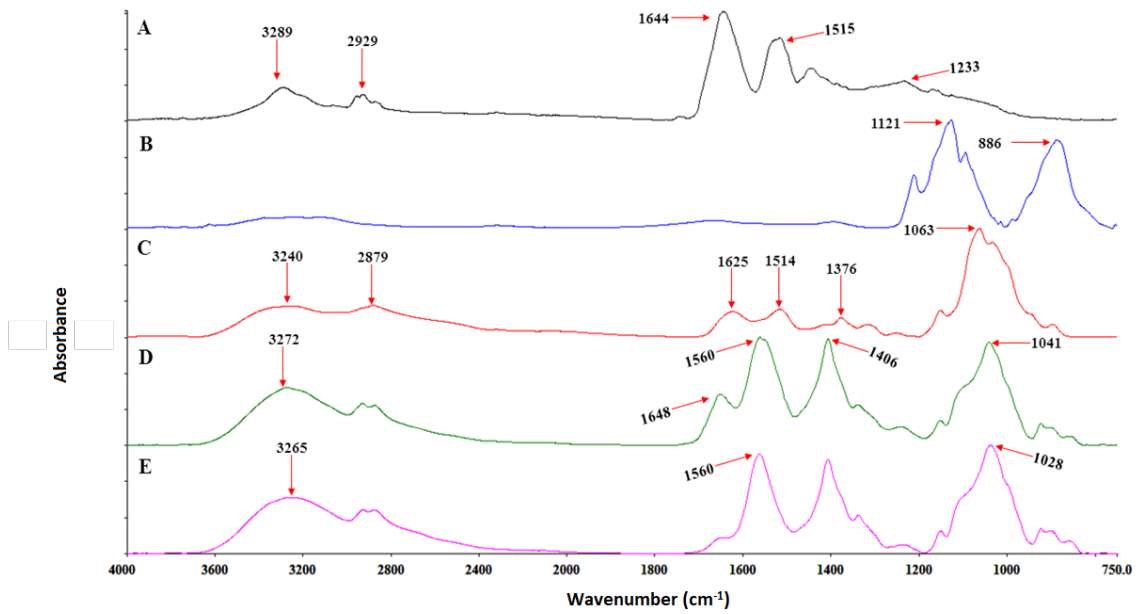
1099



1100

1101 **Figure 2**

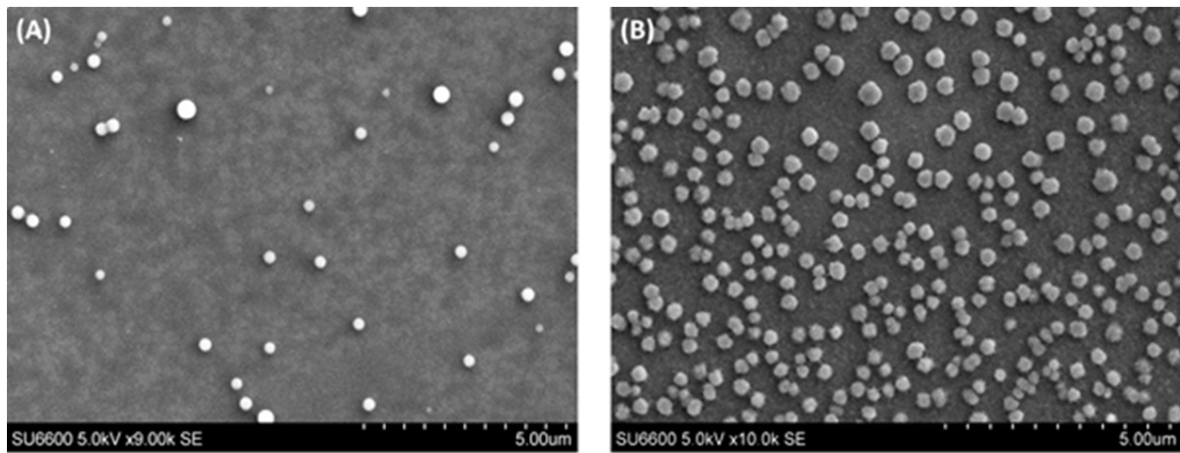
1102



1103

1104 **Figure 3**

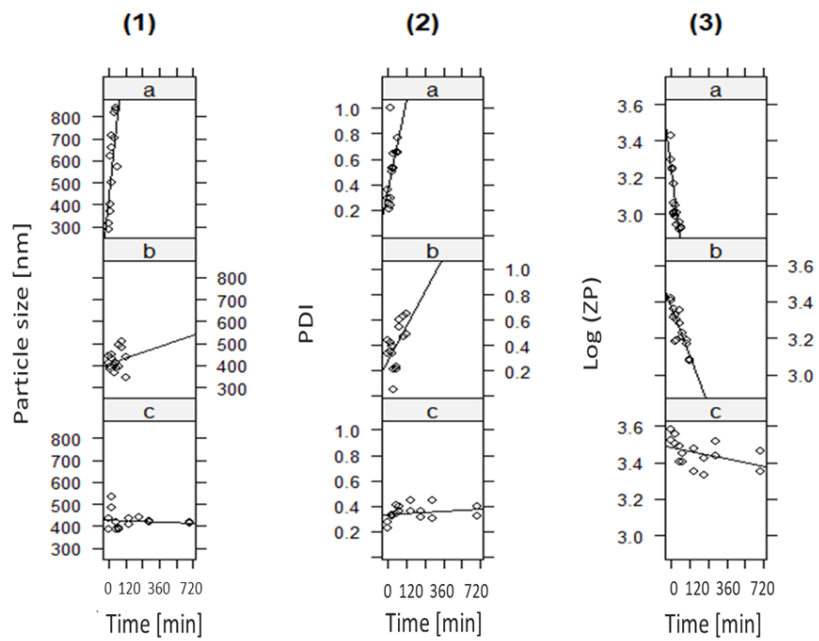
1105



1106

1107 **Figure 4**

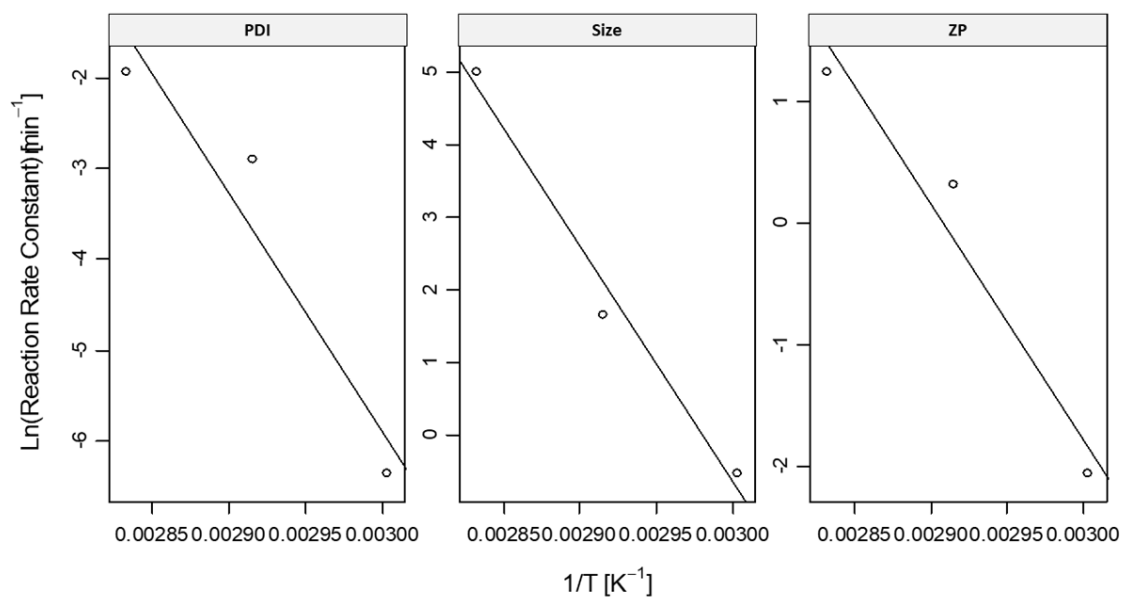
1108



1109

1110 **Figure 5**

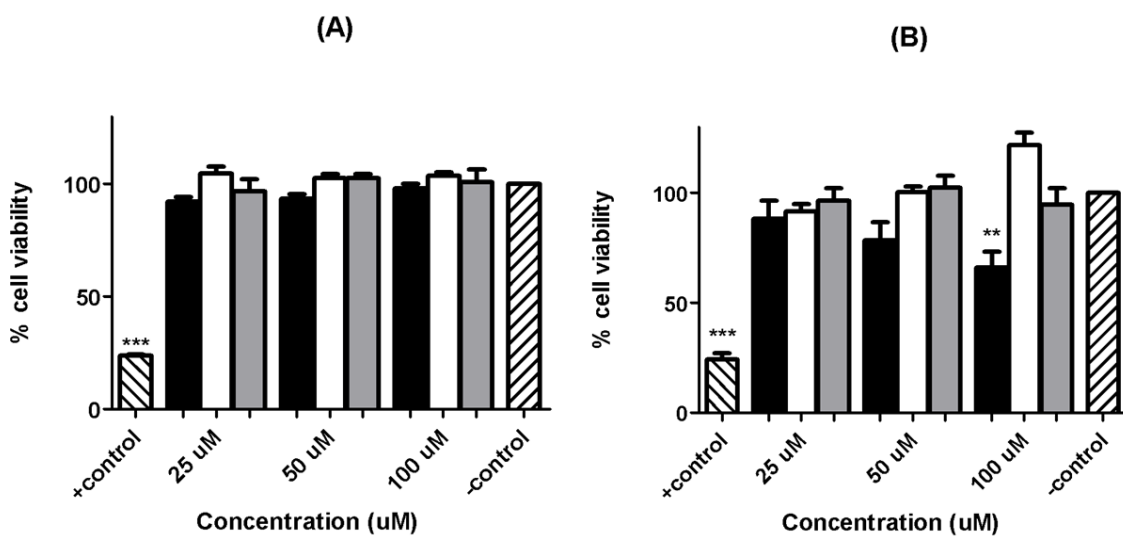
1111



1112

1113 **Figure 6**

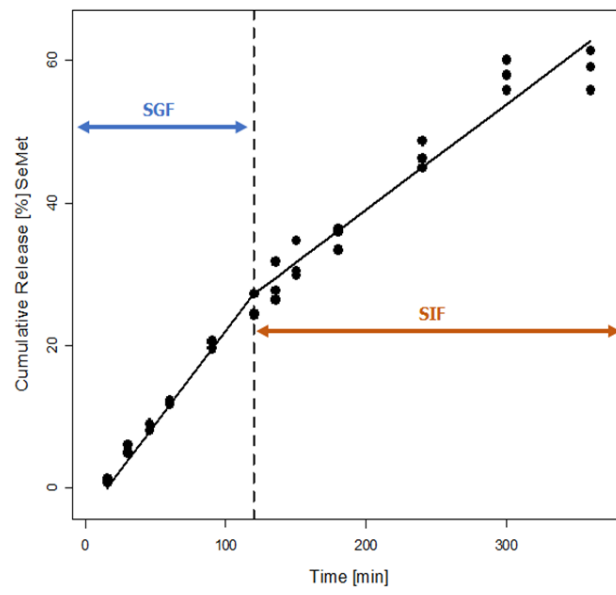
1114



1115

1116 **Figure 7**

1117



1118

1119 **Figure 8**